

# Zonal Shear Layer Collapse and The Power Scaling of The Density Limit: Old L-H Wine in New Bottles

Rameswar Singh\* and P H Diamond

*CASS, University of California San Diego, 9500 Gilman Dr,  
La Jolla, CA 92093, United States of America*

(Dated: June 2, 2022)

Edge shear layer collapse causes edge cooling and aggravates radiative effects. This paper details on the microscopic dynamics of the emergence of power ( $Q$ ) scaling of density limit from the shear layer collapse transport bifurcation scenario. The analysis is based on a novel 4-field model which evolves turbulence energy, zonal flow energy, temperature gradient and density, including the neoclassical screening of zonal flow response. Bifurcation analysis yields power scaling of critical density for shear layer collapse as  $n_{crit} \sim Q^{1/3}$ . The favorable  $Q$  scaling of the density limit emerges from the fact that the shear layer strength increases with  $Q$ , thus preventing shear layer collapse. This in turn reduces particle transport and improves particle confinement. RMP induced ambient stochastic fields degrade the shear layer by inducing decoherence in the Reynolds stress. As a result the particle transport increases and particle confinement degrades. This leads to the emergence of unfavorable stochastic field intensity ( $b_{st}^2$ ) scaling of the critical density as  $n_{crit} \sim (1 + b_{st}^2)^{-5/3}$ . All fields, including zonal flow shear, exhibit hysteresis when the power ( $Q$ ) is ramped cyclically across the bifurcation point. The hysteresis is due to dynamical delay in bifurcation on account of critical slowing down. Thus, the dynamical hysteresis here is fundamentally different from the hysteresis associated with the existence of bi-stable states.

---

\* rsingh@ucsd.edu

## I. INTRODUCTION

As this paper - “Zonal shear layer collapse and the power scaling of the density limit” - is intended for a special issue on the L-H transition, a few words of special introduction are needed. The discovery of L-H transition is indeed remarkable in that it opened a passage to good confinement[1–8]. It thereby saved magnetic confinement from wandering in the wasteland of L mode confinement. But the L-H transition brought us much more. The L-H transition introduced the ideas of transport barriers and bifurcations -i.e., the notion of stable “phases” or “states” of transport and the transitions between them. The possible changes of transport states include back transitions. The L-H transition also highlighted the role of flow profile[9] (i.e., ExB shear, etc.) in confinement, and stimulated thinking about dynamical feedback loops, predator - prey cycles, zonal flows, etc[10, 11]. More generally, contemplation of the L-H transition led us to consider the consequences of marked transport reduction. It made us aware of the need for transport regulation, not merely transport elimination.

For some time now, the existence of three phases or states of the edge plasma in tokamaks has been evident. These states are the L-mode, the H-mode, and the Density Limit state[12]. The last is a phase of stronger turbulence and degraded confinement, relative to that of L-mode[13–16]. As the Density Limit (DL) state is identified by a critical value of (line averaged) density, it is natural to think of the evolution from L-mode to DL as a kind of confinement or state transition or bifurcation, involving the edge turbulence and transport. Of course, the enhanced heat and particle transport of the DL state can lead to edge cooling, followed by multifaceted asymmetric radiation from the edge (MARFEs)[17] and MHD activity (i.e., island growth, disruption etc.)[18–20]. Indeed, these are the phenomena conventionally associated with the DL[17–20]. However, boundary transport evolution -i.e., turbulence growth, transport increase - is a necessary precursor, so as to cool the edge and degrade particle confinement. Recent experiments have indicated that degradation and collapse of the universally present L-mode shear layer[21] is the mechanism for edge confinement degradation leading to the density limit[15, 16, 22, 23]. Shear layer collapse is

signalled by a decrease in LRC(Long Range Correlation)[22] and a drop in the fluctuation driven Reynolds power as  $n \rightarrow n_G$ [15, 16]. These two are accompanied by an increase in edge particle and heat flux and a strong increase in turbulence spreading (i.e., the flux of fluctuation energy)[16]. The spreading is quasi-coherent, symptomatic of localized overturning events[24]. Analysis indicates that at the transition from L→LD, fluctuation energy is channeled from the shear layer to spreading. Note then, that the L→DL evolution has the requisite symptoms of a shear layer and confinement back transition, i.e.,

- the edge shear layer decays,
- fluctuations and transport grow,
- mesoscopic events increase.

Thus, it is rational to exploit the tools developed in the study of L→H to L→DL back transition. This explains the presence of this paper in the Special Issue.

One essential element of any transition or back transition scenario is that of a key parameter. Another is the threshold, together with its parametric dependencies. In the case of L→DL evolution, the adiabaticity parameter  $\alpha = k_{\parallel}^2 v_{the}^2 / \omega \nu$  has long been thought to be key parameter. The onset of DL phenomena is associated with the passage of  $\alpha > 1$  (adiabatic) to  $\alpha < 1$  (hydrodynamic) regimes. This evolution has been suggested as due to a possible change in turbulence type and to reduction in zonal shear production[25]. Several basic simulations[26–30] confirm this trend of finding waves and zonal flows for  $\alpha > 1$ , and 2D turbulence for  $\alpha < 1$ . The connection between a decrease in  $\alpha$  and the onset of DL has been noted in specific experiments[15, 16] and in database studies[31]. Interestingly, a recent experiment exploiting externally induced bias indicated that  $\alpha$  tends to 'follow' the evolution of ExB shear[32]. Thus,  $\alpha$  may turn out to be a “key parameter” but not a “control parameter”.

Regarding thresholds, of course density (specifically line averaged density  $\bar{n}$ ) is one threshold for the onset of DL phenomenology. The threshold density is commonly referred to as the Greenwald density[13, 33], and has long been known to scale with plasma current. Several

earlier[34–38] and recent[39] scaling studies have also suggested a power scaling as intrinsic to density limits. This power dependence emerges in high density plasma with strong auxiliary heating. Given that DL phenomenology indicates the prominent role of radiation driven phenomena[13], a scaling with power is indeed no surprise[40, 41]. However, power scaling can also enter via shear flow drive, as in the approach to the L-H transition, and so is an essential component of the shear layer collapse scenario.

In this paper, we study the connection between shear layer evolution and the L→DL threshold. Special focus is devoted to power dependence and its underlying microphysics. We identify elements of the dynamics which may be exploited to test the essentials of the theory in a way which is more rigorous than mere scaling studies are. The Kim-Diamond model[42] of L-H transition is extended to describe the evolution of turbulence intensity, zonal flow intensity, edge density and edge ion temperature gradient. The model evolves four quantities - named above - and is studied for L-mode parameters. Anticipating interest in high density regimes, we assume  $T_e = T_i$ . The mean field model is applicable to any system for electrostatic turbulence, but here we focus on the relevant case of ITG modes. Power scaling of the zonal shear layer collapse is studied by first performing a power ramp-up, followed by a density ramp-up. As density increases, the zonal flow energy decays to zero, consistent with the expectation of shear layer collapse. Note that zonal flow damping is density dependent, via collisionality. Repeating this study for a range of power reveals that the critical density for zonal flow collapse *increases* with power, suggesting a power (heat flux) scaling of the density limit. Results indicate that the scaling is  $n_{crit} \sim Q^{1/3}$ . As in previous models, current scaling of  $n_{crit}$  enters via the effect of the neoclassical dielectric[43, 44] on zonal shear evolution[45]. In addition, we show that an ambient stochastic magnetic field[46, 47] acts to lower the density limit by inducing dephasing of the Reynolds stress[48] which drives the zonal shear. This makes for a testable prediction of the effects of RMP on density limits. Analytical studies are used to illuminate the findings from numerical solution of the model.

Given the prominence of hysteresis phenomena in the L-H transition[49–53], it is natural to consider the possibility of hysteresis effects in L→DL evolution. Indeed, we will show that

all fields including zonal shear exhibit hysteresis due to critical slowing down at the L→DL back transition point. Note that hysteresis here is *not* due to bistability, as thought for the L-H transition. A detailed study of the L→DL transition dynamics is presented. Taken together, this study gives a clear, microphysical theory of the power scaling of shear layer collapse and the L-mode density limit. We also identify critical slowing down and edge heat flux hysteresis as a signature of the underlying mechanism. These studies are thus a novel and significant application of the physics learned during the study of the L-H transition.

The remainder of the paper is organized as follows. Section(II) discusses how shear layer collapse aggravates radiation effects. Section(III) presents a model of edge zonal flow collapse. In Section(IV), results from numerical studies are presented. Both scalings and hysteresis are examined. In Section(V), we show that delayed bifurcation, due to critical slowing down, is the origin of hysteresis. Section(VI) gives a Discussion and Conclusion. Aspects of the bifurcation dynamics are discussed in the Appendix(A).

## II. HOW SHEAR LAYER COLLAPSE AGGRAVATES RADIATIVE EFFECTS

Beyond a critical density, the edge shear collapses. As a result, the turbulence level increases. This in turn increases the local edge particle diffusivity  $D$  and heat diffusivity  $\chi$ .  $D$  and  $\chi$  necessarily increase upon collapse of zonal flows. As a result, the edge density and edge temperature decrease, for fixed sources. These reductions are a consequence of a transport bifurcation - i.e., a 'back transition' from a state where the shear layer coexists with turbulence, to one with no shear layer. The power loss rate due to impurity radiation is given by  $L = \sum_Z n_e n_Z L_Z(T_e)$ , where  $n_Z$  is impurity density and  $L_Z(T_e)$  cooling rate of impurity species  $Z$ , which is a function of electron temperature  $T_e$ . Reduction of edge temperature  $T_{edge}$  results in an increase in the power loss due to impurity radiation from low  $Z$  impurities (e.g. carbon). Hence, zonal flow collapse can lead to edge cooling by a sequence of shear layer collapse → increased edge transport → edge cooling → onset of radiative condensation and/or radiation - induced island growth. Note that, in this scenario, the radiative cooling is secondary to the transport bifurcation. Further increase of edge density by increasing the

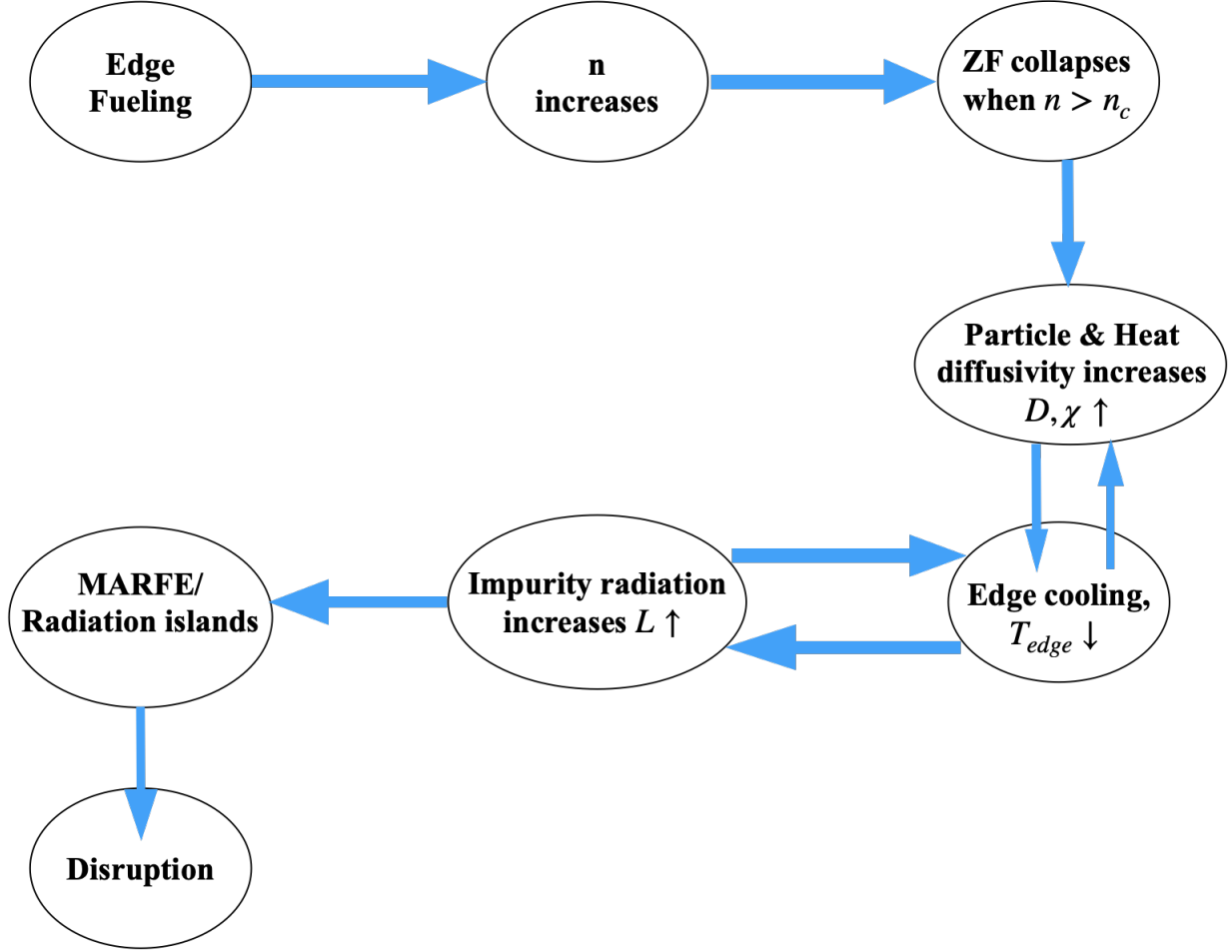


Figure 1. Schematic showing sequence of events triggered by zonal flow shear collapse leading to disruption. Enhanced transport due to zonal flow collapse can aggravate excitation of MARFE or radiation driven islands due to enhanced edge cooling, which can lead to disruption of discharge.

particle source  $S$  by intense neutral gas fueling at the edge (at fixed heating power) will cause edge cooling. Sufficiently strong cooling may trigger a MARFE[17] and or a radiation driven magnetic island[18–20], which can ultimately lead to disruption. Thus, a transport bifurcation -i.e., edge shear layer collapse may trigger undesired macroscopic phenomena in the discharge, as shown in figure(1). Higher power increases the strength of the shear layer, thus preventing the shear layer collapse. This in turn can inhibit or delay the progression of sequence of events leading to radiative density limit disruption. Thus, input power can have significant effect on the density limit. We present a model for study of power scaling of the density limit in the following section.

### III. A MODEL FOR STUDY OF EDGE ZONAL FLOW COLLAPSE

We present a  $0D$  model evolving turbulence energy  $\mathcal{E}$ , zonal flow energy  $\mathcal{E}_z$ , mean temperature gradient  $\nabla T$ , and mean density  $n$ . This minimal 4-field model is a modification of the SD21[45, 54] model which is an extension of the KD03 model of Kim and Diamond[42]. Here, the pressure equation is replaced by a temperature gradient evolution equation and an equation for the evolution of local edge density. The model is exceedingly simple. The goal here is to demonstrate zonal shear collapse scalings, explore hysteresis, including noise effects (incoherent zonal mode emission) in a clear, physically motivated way. In the following,  $\vec{q}$  refers to the wave vector for the “wavy” (or turbulent) mode and  $\vec{k} = k_x \hat{x}$  refers to the wave vector of the zonal flow. The normalized turbulence kinetic energy  $\mathcal{E} = q_y^2 \rho_s^2 I_q / q_y^2 \rho_s^2 \rho^{*2}$  evolves as:

$$\frac{\partial \mathcal{E}}{\partial t} = \underbrace{\frac{a_1 \gamma(\mathcal{N}, \mathcal{T}) \mathcal{E}}{(1 + a_3 \mathcal{V}^2)}}_{(1)} - \underbrace{a_2 \mathcal{E}^2}_{(2)} - \underbrace{\frac{a_4 \mathcal{E}_z \mathcal{E}}{(1 + b_2 \mathcal{V}^2)}}_{(3)} \quad (1)$$

Here  $t$  is the time normalized by the gyro-Bohm diffusion time i.e.,  $t \equiv t D_{GB} / a^2$ , where  $D_{GB} = c_i \rho_i \rho^*$  is the gyro-Bohm diffusivity and  $a$  is the minor radius. The first term on the right hand side represents linear growth of turbulence driven by the temperature gradient  $\mathcal{T} = -a \nabla T / T_o$  and the density gradient  $\mathcal{N} = -a \nabla n / n_o$ , via an instability with growth rate  $\gamma(\mathcal{N}, \mathcal{T})$ . The growth rate coefficient is normalized to  $a_1 \equiv a_1 a / c_i \rho^{*2}$  and the nonlinear damping rate coefficient is normalized as  $a_2 \equiv a_2 a / c_i \rho^{*2}$ . The nonlinear damping (or eddy damping) results from the triplet correlation  $\langle \phi_k \phi_p \phi_q \rangle$  as a consequence of the momentum conserving triad interaction in the turbulent kinetic energy equation[45, 54]. The factor  $\frac{1}{1 + a_3 \mathcal{V}^2}$  represents growth rate reduction by mean flow shear  $\mathcal{V}$ . The second term represents nonlinear damping of turbulence and the third term represents local damping of turbulence due to scattering of turbulence in  $k_x$ -space by mean square zonal flow shear[11]. This is a consequence of reduction in radial correlation length by mean shear. The evolution of

normalized zonal flow kinetic energy  $\mathcal{E}_z = v_z^2 = k_x^2 \rho_s^2 I_k / k_x^2 \rho_s^2 \rho^{*2}$  is governed by

$$\frac{\partial \mathcal{E}_z}{\partial t} = \underbrace{\frac{b_1 \mathcal{E} \mathcal{E}_z}{(1 + b_2 \mathcal{V}^2)}}_{(1)} - \underbrace{b_3 \hat{n} \mathcal{E}_z}_{(2)} + \underbrace{b_4 \mathcal{E}^2}_{(3)} \quad (2)$$

The first term on the right hand side represents modulational growth of zonal flow by Reynolds stress, where  $b_1 = 2(k_x^2 \rho_s^2 / \varepsilon \rho^{*2}) \left( \sum_q \Theta_{k,-q,q} c_s / a \right)$  and  $\Theta$  is triad interaction time, in dimensional form.  $\varepsilon$  is neoclassical polarization which scales quadratically with plasma current ( $I_p$ ) i.e.,  $\varepsilon \sim I_p^2$ [45]. Physically, this term represents Reynolds power. A positive Reynolds power results from the negative turbulent viscosity induced by symmetry breaking by eddy tilting by a seed ExB shear[11]. The factor  $\frac{1}{1+b_2\mathcal{V}^2}$  represents inhibition of modulational growth of zonal flow by mean flow shear[42]. This inhibition is due to the weakening of the response of drift wave spectrum to a seed zonal flow. This occurs thru the enhanced decorrelation of drift wave propagation by a mean shear flow. Note that the same suppression factor appears in the damping, due to diffusion induced by zonal flow shear, i.e.,  $a_4 = b_1$ . This guarantees conservation of total energy of turbulence and zonal flow. The second term is the linear damping of zonal flow due to collisional drag which is proportional to local density  $n$ . The third term, proportional to the square of the turbulence energy, represents the zonal noise with  $b_4 = (4/\varepsilon^2 \rho^{*2}) \sum_q q_x^2 \rho_s^2 q_y^2 \rho_s^2 \Theta(c_s/a)$ . This is a unique feature of this extension of the KD03 model. The temperature gradient  $\mathcal{T}$  evolves according to:

$$\frac{\partial \mathcal{T}}{\partial t} = - \underbrace{c_1 \frac{\mathcal{E} \mathcal{T}}{(1 + c_2 \mathcal{V}^2)}}_{(1)} - \underbrace{c_3 \mathcal{T}}_{(2)} + \underbrace{Q}_{(3)} \quad (3)$$

where the first term on the right hand side represents local damping by turbulent diffusion. The normalized turbulent damping coefficients are  $c_1 = (a/L)^2 (\chi_T / D_{GB})$  and  $c_3 = (a/L)^2 (\chi_{nc} / D_{GB})$ , where  $\chi_T$  and  $\chi_{nc}$  are turbulent and neoclassical heat diffusivities and  $D_{GB}$  is gyro-Bohm diffusivity. The factor  $\frac{1}{1+c_2\mathcal{V}^2}$  accounts for transport suppression due to (transport) cross-phase reduction by the mean flow shear[55–57]. The second term represents neoclassical transport of heat. The third term  $Q$  is a normalized source func-

tion gradient that represents input external power,  $Q = a^2 \nabla S_T / T_0 c_i \rho^{*2}$ . Here  $S_T$  is the actual temperature (i.e., heat) source function. The normalized density  $\hat{n} = n/n_0$  evolution equation is

$$\frac{\partial \hat{n}}{\partial t} = - \underbrace{d_1 \frac{\mathcal{E} \hat{n}}{(1 + d_2 \mathcal{V}^2)}}_{(1)} - \underbrace{d_3 \hat{n}}_{(2)} + \underbrace{S}_{(3)}, \quad (4)$$

where the first term on the right hand side represents local damping by turbulent diffusion. The normalized turbulent damping coefficients are  $d_1 = (a/L)^2 (D_T/D_{GB})$  and  $d_3 = (a/L)^2 (D_{nc}/D_{GB})$ , where  $D_T$  and  $D_{nc}$  are turbulent and neoclassical particle diffusivities and  $D_{GB}$  is gyro-Bohm diffusivity. The factor  $\frac{1}{1+d_2 \mathcal{V}^2}$  accounts for transport suppression due to (transport) cross-phase reduction by the mean flow shear[55, 56]. The second term represents neoclassical transport of density. The third term  $S$  is the normalized particle source function that represents input external source,  $S = a S_n / n_0 c_i \rho^{*2}$ . Here  $S_n$  is the dimensional particle source function. The meaning of different terms in the model equations(1), (2), (3) and (4) are summarized in table(I). Finally, the normalized mean flow shear  $\mathcal{V} \equiv V'_E a / \rho^* c_i$  is related to the temperature gradient  $\mathcal{T}$ , the density gradient  $\mathcal{N}$  and the local density  $n$  through the diamagnetic part of radial force balance

$$\mathcal{V} \equiv \frac{V'_E a}{\rho^* v_{thi}} = -\frac{1}{\hat{n}} \mathcal{N} \left( \frac{1}{\hat{n}} \mathcal{N} + \frac{1}{\hat{T}} \mathcal{T} \right). \quad (5)$$

Here couplings to mean poloidal and toroidal flows are ignored for simplicity.  $\hat{T} = T/T_0$  is normalized local temperature. Note that this model is an outgrowth of, and yet different from, the KD03 model, in the sense that it considers the effect of zonal noise, and also includes the effect of mean  $E \times B$  induced suppression of turbulence growth, and modulational zonal growth and transport cross-phase reduction. Density gradient  $\mathcal{N}$  and local temperature  $\hat{T}$  are not evolved. Notice the neoclassical polarization dependence of the modulational growth parameter ( $b_1 \sim \varepsilon^{-1} \sim I_p^2$ ), the zonal noise parameter ( $b_4 \sim \varepsilon^{-2} \sim I_p^4$ ), and the density dependence of  $\gamma$ , zonal flow damping rate  $b_3$ , and the mean  $E \times B$  flow shear  $\mathcal{V}$ . These features make this model suitable for the study of the scalings of zonal collapse.

The model yield power and current scalings of the density limit for shear layer collapse. Sensitivity of the scalings to the type of turbulence can be studied by adopting different expressions for  $\gamma$ . Here, we assume that the turbulence is dominated by the toroidal ion temperature gradient (ITG) driven modes.

Terms→ Equations ↓	(1)	(2)	(3)
Turbulence energy $\mathcal{E}$ -eqn	Linear growth with reduction factor $\frac{1}{1+a_3\mathcal{V}^2}$ due to mean ExB shear.	Non-linear damping.	Local damping due to scattering of turbulence in $k_x$ -space by mean square zonal flow shear with inhibition in forward transfer by mean ExB shear. $a_4 = b_1 \sim I_p^2$
Zonal flow energy $\mathcal{E}_z$ -eqn	Symmetry breaking by eddy tilting by seed ExB shear induces a turbulent negative viscosity effect, which excites zonal flow by modulational instability. Inhibition of modulational growth by mean shear (captured by factor $\frac{1}{1+b_2\mathcal{V}^2}$ ) reflects as reduction in local damping of turbulence due to forward scattering in $k_x$ -space. $b_1 \sim I_p^2$	Collisional damping of zonal flow $\sim n$ .	Zonal noise due to incoherent mode coupling . $b_4 \sim I_p^4$
Temperature gradient $\mathcal{T}$ -eqn	Turbulent heat transport with reduction factor $\frac{1}{1+c_2\mathcal{V}^2}$ due to cross phase reduction due to mean ExB shear.	Neoclassical heat transport.	Input heat source. (Control parameter)
Density $\hat{n}$ -eqn	Turbulent particle transport with reduction factor $\frac{1}{1+d_2\mathcal{V}^2}$ due to cross phase reduction due to mean ExB shear.	Neoclassical particle transport.	Particle source. (Control parameter)

Table I. Meaning of different terms in model equations(1), (2), (3) and (4).

## IV. RESULTS FROM NUMERICAL EXPERIMENTS OF THE MODEL: SCALINGS AND HYSTERESIS

### A. Power scaling of shear layer collapse and density limit

The model equations(1), (2), (3), (4) and (5) are integrated numerically. The results are described in this section. Figure(2) shows the temporal evolution of the turbulence energy  $\mathcal{E}$ , zonal flow energy  $\mathcal{E}_z$ , normalized temperature gradient  $\mathcal{T}$  and normalized density  $\hat{n}$  in a sequence of a ramp of input power  $Q$  followed by a ramp of the particle source  $S$ . The input power is ramped up and kept steady at a level well below the L-H threshold power so as to study zonal flow dynamics in the L mode. The temporal evolution of  $\mathcal{E}$ ,  $\mathcal{E}_z$  and  $\mathcal{T}$  of the 4-field system (zonal noise parameter  $b_4 = 0$ ) during the power ramp up phase is qualitatively similar to that of the KD03 model[42]. Different stages of evolution of the system in time are described as follows:

- As the input power  $Q$  ramped up from zero, the mean temperature gradient  $\mathcal{T}$  steepens and excites turbulence by linear instability.
- Upon further heating, turbulence continues to grow and excites zonal flows when the input power exceeds a threshold set by the turbulence level and flow damping. When the turbulent drive becomes strong enough to overcome flow damping, it generates zonal flows by Reynolds stress. The turbulence energy overshoots dramatically before the growth of the zonal flow. Turbulence and zonal flows then form a self-regulating system, since the shearing by zonal flows damps the turbulence. Zonal flows and turbulence compete, and oscillatory behavior emerges.
- A gradual increase of both the turbulence energy and the zonal flow energy occurs while continuing the heating ramp after the first appearance of zonal flow. This is due to the reduction in the zonal flow growth by the mean shear flow, which in turn strengthens the growth of turbulence. The behavior of the turbulence envelope after zonal flow excitation is given by the stationary solution of equation(2) i.e  $\mathcal{E} = b_3 \hat{n} (1 + b_2 \mathcal{V}^2) / b_1$ ,

which increases as the pressure gradient increases with  $Q$ . The increase of saturated turbulence energy with  $Q$  is due to dephasing of Reynolds stress by the mean shear. Reynolds stress dephasing by mean  $E \times B$  shear lowers the modulational growth rate i.e.,  $b_1 \rightarrow b_1/(1 + b_2\mathcal{V}^2)$ . This in turn saturates the turbulence energy at a higher level. The envelope of the zonal flow is given by the stationary solution of the equation(1) i.e.,

$$\mathcal{E}_z = \frac{a_2}{a_4} (1 + b_2\mathcal{V}^2) \left[ \frac{a_1}{a_2} \frac{\gamma}{(1 + b_2\mathcal{V}^2)} - \frac{b_3}{b_1} \hat{n} (1 + b_2\mathcal{V}^2) \right]. \quad (6)$$

Clearly, *the steady state zonal flow energy is affected not only by the density but also by the input power which determines the mean  $E \times B$  shear.* At low power, mean  $E \times B$  shear is weak such that  $\frac{a_1}{a_2}\gamma \gg \frac{b_3}{b_1}\hat{n}(1 + b_2\mathcal{V}^2)^2$ , and the zonal flow energy increases with input power. Power and density compete to set the level of zonal flow energy. Hence a power scaling of the density limit exists.

- To study the power scaling of the density limit set by zonal shear collapse, the following strategy is adopted. First, the particle source is kept steady and the power is ramped up until a desired level of zonal flow is achieved. The power is then held steady and after a time lag, the particle source is ramped up. As the plasma density rises, the zonal flow energy begins to decrease due to enhanced collisional damping. As a result, the turbulence energy increases with the source ramp up. At large enough density the zonal flow energy drops to zero (i.e.,  $\mathcal{E}_z = 0$ ) and the turbulence energy becomes steady at the value

$$\mathcal{E} = \frac{a_1}{a_2} \frac{\gamma}{(1 + b_2\mathcal{V}^2)} \quad (7)$$

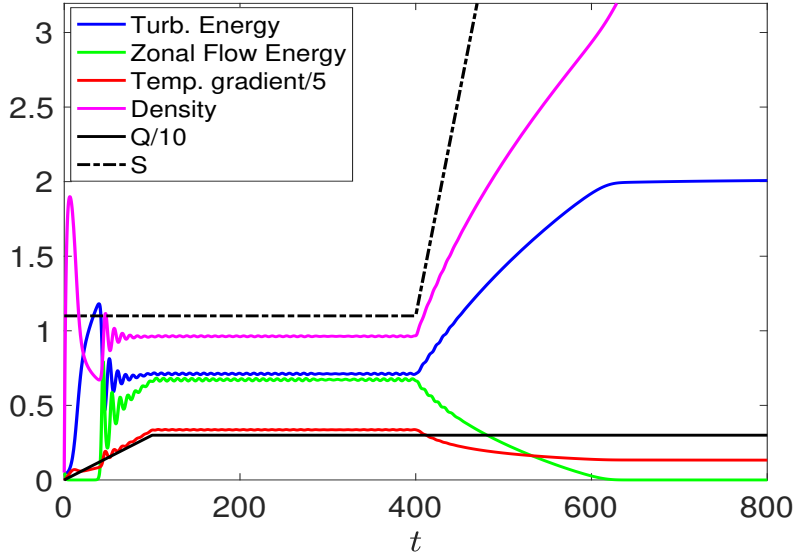


Figure 2. Time evolution of turbulence energy, zonal flow energy, density and temperature gradient in a successive power and density ramp. Parameters:  $a_1 = 1$ ,  $a_2 = 0.2$ ,  $a_3 = 0.7$ ,  $a_4 = 0.7$ ,  $b_1 = 1.5$ ,  $b_2 = 0.7$ ,  $b_3 = 1$ ,  $b_4 = 0$ ,  $c_1 = 2$ ,  $c_2 = 0.5$ ,  $d_1 = 1$ ,  $d_2 = 0.5$ ,  $\sqrt{\beta} = 0.05$ ,  $S(t) = 1.1 + 0.03(t - 400)\Theta(t - 400)$ ,  $Q(t) = 0.03t\Theta(100 - t) + 3\Theta(t - 100)$ . See description in the text.

The numerical experiment just described is then repeated for higher powers. The zonal flow and turbulence energy evolution for different powers are shown in Figure(3). The source ramp is the same for all cases. *The zonal flow level increases with input power.* It can be seen that at higher power, it takes a longer time for the zonal flow to damp -i.e., the density must ramp up further. This means that the critical density for the zonal flow collapse *increases* with input power. Notice that in the zonal flow collapse regime, the saturated turbulence energy also increases with power at a rate larger than that in the finite zonal flow regime. This is because of channeling of input power to the zonal flows via turbulence in the latter.

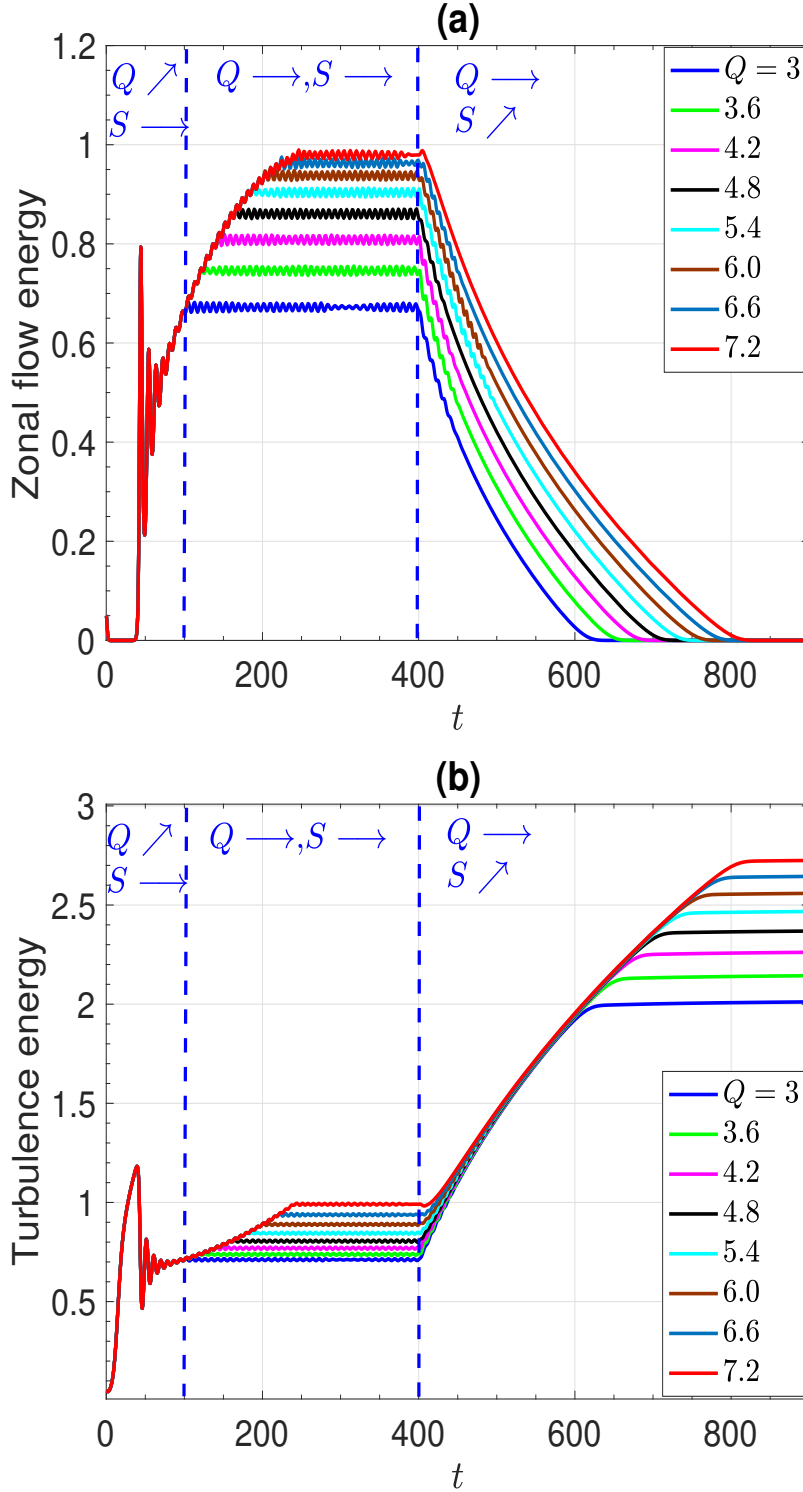


Figure 3. (a): Zonal flow energy damping with particle source  $S$  ramp up at different powers  $Q$ . The zonal flow damping time increases with the input power. Clearly, the critical density for the zonal flow collapse increases with the input power. (b): Turbulence energy evolution in successive  $Q$  and  $S$  ramp. Other parameters same as in figure(2). Diagonal arrow means ramp up and right arrow means steady.

The critical densities obtained from the numerical initial value experiment and the static bifurcation analysis (for increasing power) are plotted in figure(4). It can be seen that both initial value analysis and a static bifurcation analysis yield a critical density which scales with the power as  $n_{crit} \sim Q^{1/3}$ . However, the absolute value of the  $n_{crit}$  obtained from the initial value analysis is larger than that the  $n_{crit}$  obtained from the static bifurcation analysis. This is due to dynamical delay in bifurcation caused by “critical slowing down” effect at the static bifurcation point. Finally, Zanca’s fit[41] using a radiative power balance model is shown for comparison. Our model based on zonal shear collapse paradigm yields a somewhat milder power scaling than the radiative power balance model i.e.,  $Q^{1/3}$  vs  $Q^{4/9}$ .

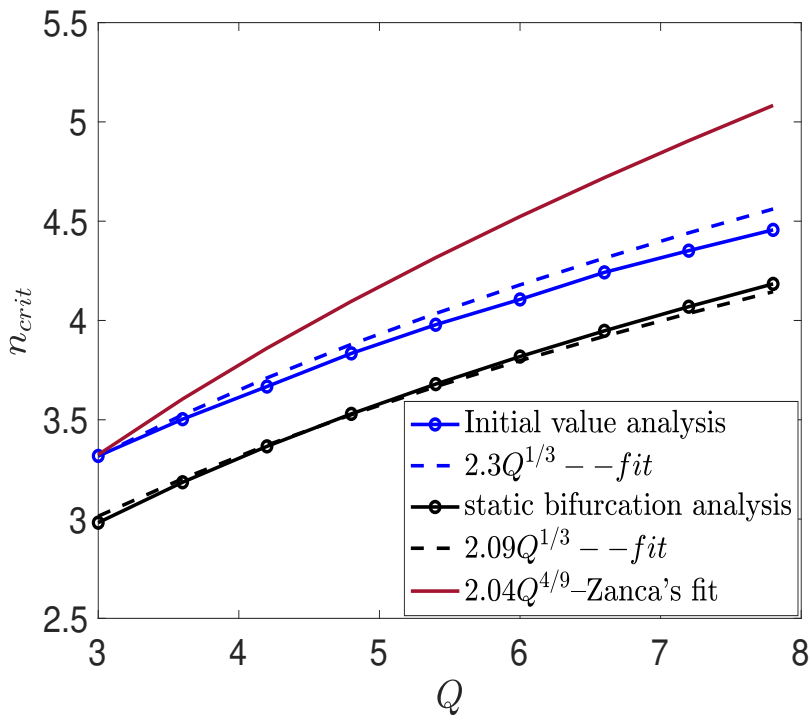


Figure 4. Power scaling of the critical density for zonal flow collapse for the toroidal ITG case. Initial value analysis yields higher critical density for zonal flow collapse due to critical slowing down at static bifurcation point. The critical density in the initial value analysis correspond to the zonal flow energy level  $\mathcal{E}_z = 10^{-5}$ .

1. *Understanding power scaling of the critical density*

The linear growth rate of toroidal ITG turbulence, in dimensional form, is

$$\gamma = f \sqrt{\frac{R}{L_T} - \left(\frac{R}{L_T}\right)_{crit}} \quad (8)$$

where  $f = \frac{|k_y \rho_s^2|}{1+k_\perp^2 \rho_s^2} \left(2\frac{T_i}{T_e}\right)^{1/2} \frac{c_s}{R}$  and  $\left(\frac{R}{L_T}\right)_{crit} = \frac{R}{L_n} \eta_{th} = \frac{R}{L_n} \left(\frac{2}{3} - \frac{1}{2\tau_i}\right) + \frac{1}{8\tau_i} \left(\frac{R}{L_n}\right)^2 + 2\left(\frac{1}{4\tau_i} + \frac{10}{9\tau_i}\right)$  is the critical temperature gradient scale length. This expression for the growth rate results from a local interchange type model of ITG turbulence in the strong ballooning limit, assuming adiabatic electrons and ignoring the parallel ion dynamics[58, 59]. Note that, this simplified expression of the linear growth rate does not capture the most accurate form of  $k_y$  dependence obtained from the gyrokinetic calculations[60]. However, this does not matter for the power scaling of the density limit. In fact, it is the nature of the temperature gradient dependence of the linear growth rate that decides the power scaling of the density limit for shear layer collapse. This is because of channelling of applied power to the zonal flows via the turbulence. The numerical results were obtained assuming a threshold  $\left(\frac{R}{L_T}\right)_{crit} = \frac{R}{L_n} \eta_{th} = 0.5\frac{R}{L_n}$ , for simplicity. From the zonal flow energy envelope equation(6), and ignoring the mean  $E \times B$  shear feedback effect, the zonal flow collapse criterion can be obtained as

$$\frac{\gamma_d}{b_1} > \frac{a_1 \gamma}{a_2}$$

where  $\gamma_d = b_3 \hat{n}$  is zonal flow damping rate,  $b_1$  is modulational growth rate,  $\gamma$  is linear turbulence growth rate and  $a_2$  is non-linear damping rate. Assuming the critical temperature gradient  $\left(\frac{R}{L_T}\right)_{crit} = 0$  for simplicity,

$$\left(\frac{\gamma_d}{b_1}\right)^2 > \left(\frac{a_1 f}{a_2}\right)^2 \frac{R}{L_T}$$

Using the power balance, and ignoring the neoclassical heat flux i.e.,  $-\chi \frac{dT}{dx} = Q$

$$\left(\frac{\gamma_d}{b_1}\right)^2 > \left(\frac{a_1 f}{a_2}\right)^2 \frac{RQ}{\chi T}$$

Here  $\chi$  is turbulent heat diffusivity which scales linearly with turbulence energy  $\chi = \chi_0 \mathcal{E}$ . For the relevant case of saturation by zonal flows, the turbulence energy is given by  $\mathcal{E} = \gamma_d/b_1$ . Hence we obtain the zonal flow collapse criterion:

$$\left(\frac{\gamma_d}{b_1}\right)^3 > \left(\frac{a_1 f}{a_2}\right)^2 \frac{RQ}{\chi_0 T}$$

Finally, recall that the collisional zonal flow damping  $\gamma_d \sim n$  and the modulational growth coefficient  $b_1 \sim I_p^2$ . This yields a critical density  $n_{crit}$  for zonal flow collapse, which scales with power and plasma current as:

$$n_{crit} \sim I_p^2 Q^{1/3} \quad (9)$$

Thus the critical density increases with the input power. The zonal flow energy increases with the input power. This, in turn, requires higher density for the zonal flow collapse. This is the physical mechanism underlying the power dependence. This explains the  $Q$  dependence of the critical density plotted in figure(4), obtained from numerical initial value analysis. How does turbulence energy scale with power after the zonal flow collapse? From equation(7) and (8), ignoring the mean shear feedback, one can get

$$\mathcal{E}^2 = \left(\frac{a_1 f}{a_2}\right)^2 \frac{R}{L_T} \quad (10)$$

Again, using the power balance and ignoring the neoclassical heat flux i.e.,  $-\chi \frac{dT}{dx} = Q$

$$\mathcal{E}^2 = \left(\frac{a_1 f}{a_2}\right)^2 \frac{RQ}{\chi T} \quad (11)$$

Noting that the turbulent heat diffusivity which scales with  $\mathcal{E}$  as  $\chi = \chi_0 \mathcal{E}$ , the above equation becomes

$$\mathcal{E} = \left( \frac{a_1 f}{a_2} \right)^{2/3} \left( \frac{RQ}{\chi_0 T} \right)^{1/3} \quad (12)$$

i.e., after the zonal shear collapse the turbulence intensity scales with power as

$$\mathcal{E} \sim Q^{1/3} \quad (13)$$

Thus turbulence energy in the zonal flow collapsed state increases with the input power, as seen in figure(3).

### B. Scaling with Stochastic fields

Resonant magnetic perturbation, applied to mitigate edge localized modes, makes the resultant 3D magnetic field stochastic[46]. The stochasticity results when the magnetic islands localized at the resonant surfaces overlap. Here we study the effect of ambient stochastic fields on zonal flow dynamics. For this purpose, we extend the model described in section(III) according to the results obtained in Ref[48]. The modifications in the model due to the stochastic fields appear through the linear growth rate of turbulence, modulational growth rate of zonal flow, heat and particle fluxes. Again, the modifications are simple but physics guided, which facilitate study zonal flow collapse dynamics in the presence of ambient stochastic fields. The linear growth rate factor is modified as  $\gamma \rightarrow \gamma/(1 + b_{st}^2)$ . Here  $b_{st}^2 = q \left| \frac{\delta B_r}{B} \right|^2 / \sqrt{\beta} \rho_*^2 \epsilon$  is normalized magnetic fluctuation intensity.  $q$  is safety factor,  $\beta$  is plasma beta defined as the ratio of plasma kinetic pressure to magnetic pressure,  $\epsilon$  is aspect ratio and  $\delta B_r$  is a radial magnetic field perturbation. This is in accordance with recent theory and simulations that stochastic fields reduce the linear growth rate of turbulence[48, 61, 62]. The modulational growth coefficient of the zonal flow is modified as  $b_1 \rightarrow b_1/(1 + b_{st}^2)$ . This is in accordance with the fact that the stochastic fields decrease the Reynolds stress by dephasing it. The turbulent heat and diffusivity coefficients are modified  $c_1 \rightarrow c_1/(1 + b_{st}^2 \sqrt{\beta})$

and  $d_1 \rightarrow d_1/(1 + b_{st}^2\sqrt{\beta})$  respectively. This modification accounts for the decoherence of the turbulent heat and particle fluxes by the ambient stochastic magnetic fields. Notice that here it is smaller by amount  $\sqrt{\beta}$  (i.e.,  $b_{st}^2 \rightarrow b_{st}^2\sqrt{\beta}$ ) due to the fact that acoustic wave scattering is what causes decoherence[48].

The extended model with the stochastic field effects is integrated numerically. The results are discussed in the following. The zonal flow and turbulence energy evolutions at different stochastic field intensities are plotted in figure(5), for fixed power and a source ramp. The threshold power for zonal flow excitation increases with the stochastic field amplitude. The zonal flow energy decreases and turbulence energy increases upon increasing the stochastic field intensity in the steady power and source region. The behavior of the turbulence envelope after zonal flow excitation is given by  $\mathcal{E} = b_3\hat{n} (1 + b_2\mathcal{V}^2) (1 + b_{st}^2)/b_1$ . The envelope of the zonal flow is given by

$$\mathcal{E}_z = \frac{a_2}{a_4} (1 + b_2\mathcal{V}^2) \left[ \frac{a_1}{a_2} \frac{\gamma}{(1 + b_2\mathcal{V}^2)} - \frac{b_3}{b_1} \hat{n} (1 + b_2\mathcal{V}^2) (1 + b_{st}^2)^2 \right]. \quad (14)$$

Upon source ramp up, the zonal flow energy decreases and turbulence energy increases. Notice that the time for zonal flow decay decreases with increasing stochastic field intensity. This means that the critical source (and hence the critical density) for zonal flow collapse *decreases* with the stochastic field intensity. After zonal flow collapse, the saturated turbulence energy decreases with stochastic field amplitude. In the zonal flow collapsed state (i.e.,  $\mathcal{E}_z = 0$ ), the turbulence saturates by the balance of linear growth and nonlinear damping. Here the envelope level of turbulence energy is given

$$\mathcal{E} = \frac{a_1}{a_2} \frac{\gamma}{(1 + b_{st}^2)(1 + b_2\mathcal{V}^2)} \quad (15)$$

. Decrease of the turbulence energy by stochastic fields after the zonal flow collapse is due to a reduction in linear growth by stochastic fields.

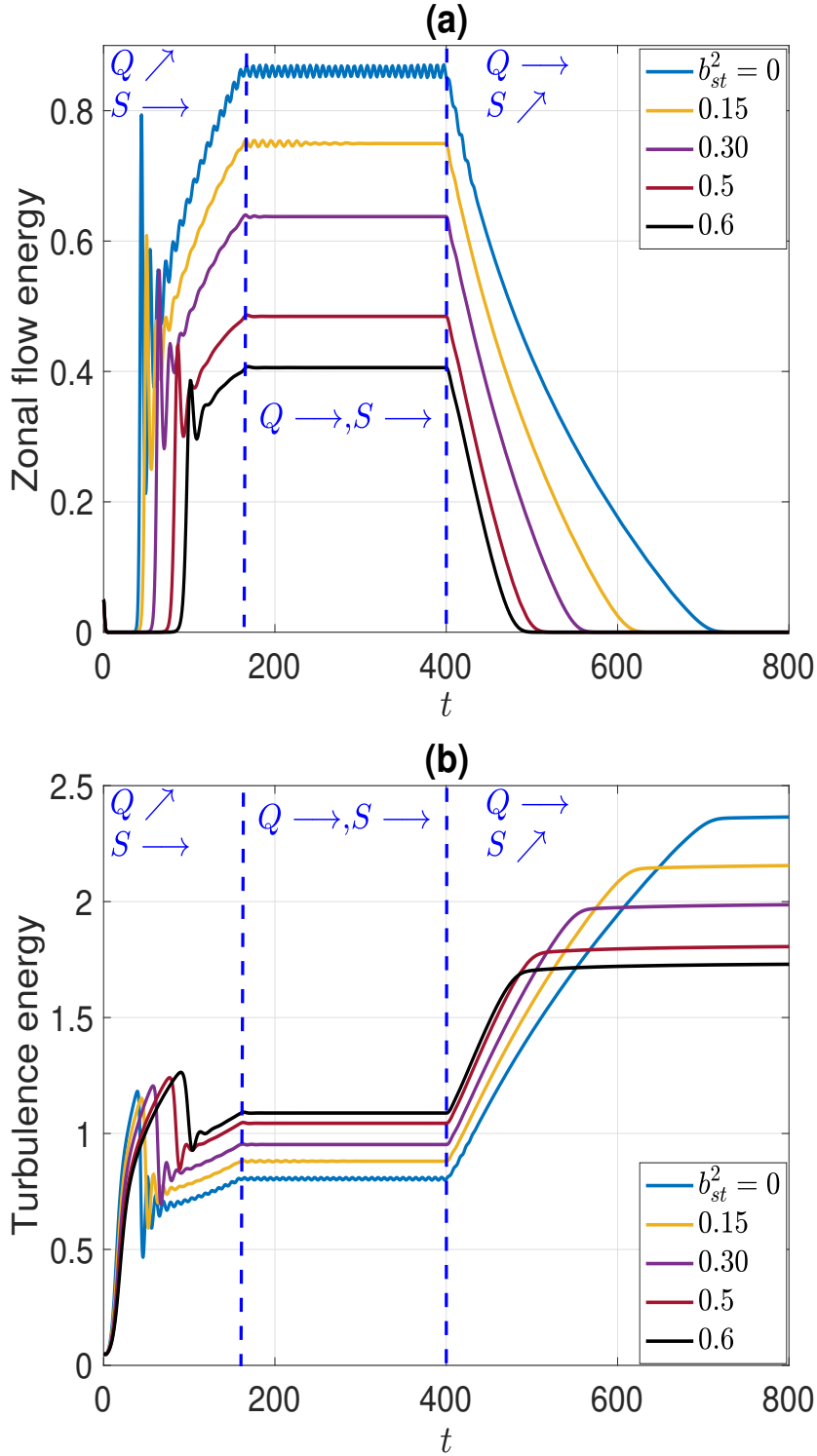


Figure 5. Zonal flow energy (a) and turbulence energy (b) evolution in a successive ramp of input power  $Q$  and particle source  $S$  for different values of the normalized stochastic field intensity  $b_{st}^2 = q \left( \frac{\delta B_r}{B} \right)^2 / \sqrt{\beta} \rho_*^2 \epsilon$ . Power is ramped up to  $Q = 4.8$ . Notice that the zonal flow collapse is accelerated by the stochastic fields. Diagonal arrow means ramp up and right arrow means steady.

Figure(6) shows that critical density for zonal shear collapse *decreases* with the stochastic magnetic field amplitude. The critical density scales with the stochastic magnetic field as  $n_{crit} \sim (1 + b_{st}^2)^{-5/3}$ . This is a *testable prediction* which calls for a density limit experiment with RMPs in L mode.

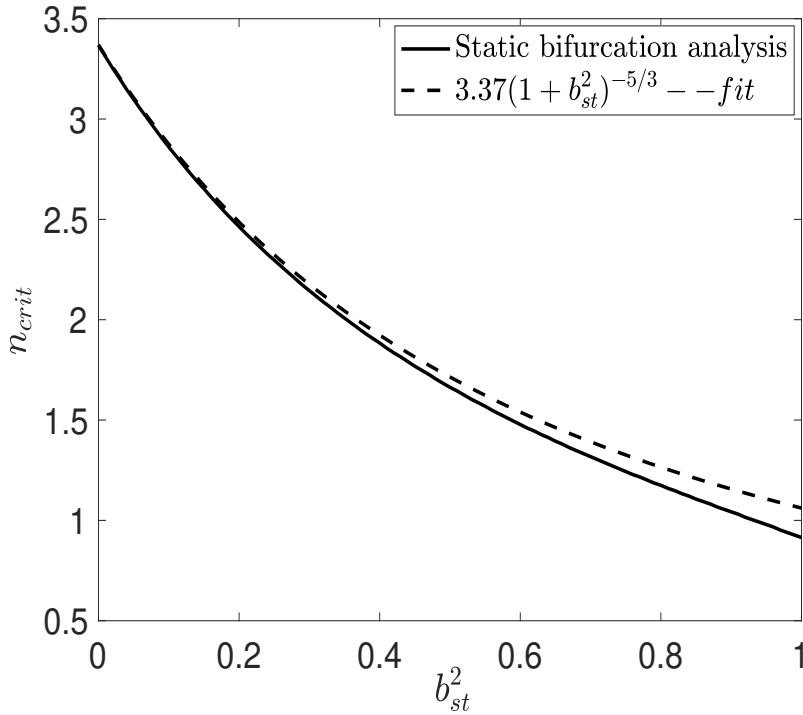


Figure 6. Stochastic field intensity  $b_{st}^2 = q \left( \frac{\delta B_r}{B} \right)^2 / \sqrt{\beta} \rho_*^2 \epsilon$  scaling of the critical density for zonal flow collapse, obtained from static bifurcation analysis.

### 1. Understanding the stochastic field scaling of the critical density

From the zonal flow energy envelope equation(14), and ignoring the mean  $E \times B$  shear effect, the zonal flow collapse criterion can be obtained as

$$\frac{\gamma_d}{b_1} (1 + b_{st}^2)^2 > \frac{a_1 \gamma}{a_2} \quad (16)$$

where  $\gamma_d = b_3 \hat{n}$  is zonal flow damping rate,  $b_1$  is modulational growth rate,  $\gamma$  is linear turbulence growth rate and  $a_2$  is non-linear damping rate. Assuming the critical temperature gradient  $\left(\frac{R}{L_T}\right)_{crit} = 0$  for simplicity,

$$\left(\frac{\gamma_d}{b_1}\right)^2 (1 + b_{st}^2)^4 > \left(\frac{a_1 f}{a_2}\right)^2 \frac{R}{L_T} \quad (17)$$

Using the power balance, and ignoring the neoclassical heat flux i.e.,  $-\chi \frac{dT}{dx} = Q$

$$\left(\frac{\gamma_d}{b_1}\right)^2 (1 + b_{st}^2)^4 > \left(\frac{a_1 f}{a_2}\right)^2 \frac{RQ}{\chi T} \quad (18)$$

Here  $\chi$  is turbulent heat diffusivity which scales linearly with turbulence energy  $\chi = \chi_0 \mathcal{E} / (1 + b_{st}^2 \sqrt{\beta})$ . For the relevant case of saturation by zonal flows the turbulence energy is given by  $\mathcal{E} = \gamma_d (1 + b_{st}^2) / b_1$ . Hence we obtain the zonal flow collapse criterion

$$\left(\frac{\gamma_d}{b_1}\right)^3 (1 + b_{st}^2)^5 > \left(\frac{a_1 f}{a_2}\right)^2 \frac{RQ}{\chi_0 T} (1 + b_{st}^2 \sqrt{\beta}) \quad (19)$$

Finally, recall that  $\gamma_d \sim n$  and  $b_1 \sim I_p^2$ , so this yields a critical density  $n_{crit}$  for zonal flow collapse, which scales with power and plasma current and stochastic field intensity as

$$n_{crit} \sim I_p^2 Q^{1/3} \frac{(1 + b_{st}^2 \sqrt{\beta})^{1/3}}{(1 + b_{st}^2)^{5/3}} \quad (20)$$

Thus, the critical density for the zonal flow collapse *decreases* with the increasing stochastic magnetic field intensity. Stochastic fields erode the zonal flow shear by dephasing the Reynolds stress. As a result the critical density for zonal flow collapse is reduced. The particle transport increases and particle confinement degrades. Ambient stochastic fields accelerate the shear layer collapse when density is increased. This explains the scaling trend of  $n_{crit}$  with  $\alpha$  shown in figure(6). How does turbulence energy scale with stochastic field intensity after the zonal flow collapse? From equation(15) and (8), ignoring the mean shear feedback, one can get

$$\mathcal{E}^2 = \left(\frac{a_1 f}{a_2}\right)^2 \frac{\frac{R}{L_T}}{(1 + b_{st}^2)^2} \quad (21)$$

Using the power balance, and ignoring the neoclassical heat flux,

$$\mathcal{E}^2 = \left( \frac{a_1 f}{a_2} \right)^2 \frac{\frac{RQ}{\chi T}}{(1 + b_{st}^2)^2} \quad (22)$$

Noting that the turbulent heat diffusivity scales with  $\mathcal{E}$  and  $b_{st}^2$  as  $\chi = \chi_0 \mathcal{E} / (1 + b_{st}^2 \sqrt{\beta})$ , the above equation becomes

$$\mathcal{E} = \left( \frac{a_1 f}{a_2} \right)^{2/3} \frac{\left( \frac{RQ}{\chi_0 T} \right)^{1/3} (1 + b_{st}^2 \sqrt{\beta})^{1/3}}{(1 + b_{st}^2)^{2/3}} \quad (23)$$

i.e., after the zonal shear collapse the turbulence intensity scales with stochastic field as

$$\mathcal{E} \sim \frac{1}{(1 + b_{st}^2)^{2/3}}. \quad (24)$$

Notice the reversal of trend of turbulence energy with respect to the stochastic field intensity after the zonal flow collapse. Before the zonal flow collapse, the turbulence energy scales as  $\mathcal{E} \sim (1 + b_{st}^2)$  i.e., turbulence energy increases with increasing  $\alpha$ . This is because of reduction of zonal flow energy due to dephasing of the Reynolds stress by the stochastic magnetic fields. Whereas, after the zonal flow collapse the turbulence energy scales as  $\mathcal{E} \sim (1 + b_{st}^2)^{-2/3}$  i.e., turbulence energy decreases with increasing  $\alpha$ . This is because of linear growth rate reduction by stochastic magnetic field i.e.,  $\gamma \rightarrow \gamma / (1 + b_{st}^2)$ . This explains the turbulence energy behavior with respect to the stochastic field intensity shown in figure(5).

### C. Hysteresis with cyclic power $Q$ ramp

Above numerical and theoretical analysis convinced that shear layer bifurcation physics is the key to emergence of power scaling of the density limit. Hysteresis is a dynamical manifestation of bifurcation phenomenon when the control parameter is varied across a bifurcation point. For example, L-H hysteresis appears when input power is ramped back and forth across the L-H power threshold (i.e., the bifurcation point). The system jumps from one stable state(L-mode) to another stable state (H-mode) in a Hopf bifurcation. So

hysteresis is symptomatic of a transport bifurcation process. One wonders whether the transport bifurcation leading to zonal shear collapse is hysteretic? To address this question another set of numerical experiments are performed with a cyclic source  $S$  function. The results are described in detailed in Appendix(A). The results show that the hysteresis with a cyclic  $S$  is *drastically* reduced by the zonal noise. Hence, hysteresis with cyclic  $S$  *may not* be observed in experiments. Also, ramping  $S$  cyclically may be more challenging than ramping  $Q$  in experiments. Realizing that the zonal flow hysteresis in  $S$  ramp may not be observable in a realistic situation with zonal noise, the possibility of hysteresis is investigated for the case of a cyclic power  $Q$  ramp. The results without the zonal noise are plotted in figure(7). The left panel of figure(7) shows the time evolution of turbulence energy, zonal flow energy, temperature gradient, and the density when the input power  $Q$  is ramped periodically, while the particle source  $S$  remains fixed. The range of variation of  $Q$  is such that it remains well below the L-H power threshold. The following are the striking features of this plot: both turbulence and zonal flow energies increase with increasing  $Q$ , and decrease with decreasing  $Q$ . However, the temporal structure of any field is not symmetric about the time when the  $Q$  is maximum in a triangular heat pulse, e.g., for a triangular  $Q$  pulse duration  $t = [200, 400]$ , the system has broken  $t$ -symmetry about the time  $t = 300$ . This implies that all fields are hysteretic in  $Q$ . The right panel of figure(7) shows hysteresis of turbulence and zonal flow energies plotted in time interval  $t = [200, 400]$ . Notice that zonal flow appears at powers higher than the static bifurcation point. The static bifurcation point is the cross-over point where the two bifurcation curves exchange their stability. This delay in the forward and the backward bifurcation leads to appearance of zonal flow hysteresis. It should be clear that there is only one stable fixed point at any  $Q$ , given by equations(A1) and (A2). So the hysteresis observed here is not due to static bistability, but due to dynamic delay caused by critical slowing down at the bifurcation point.

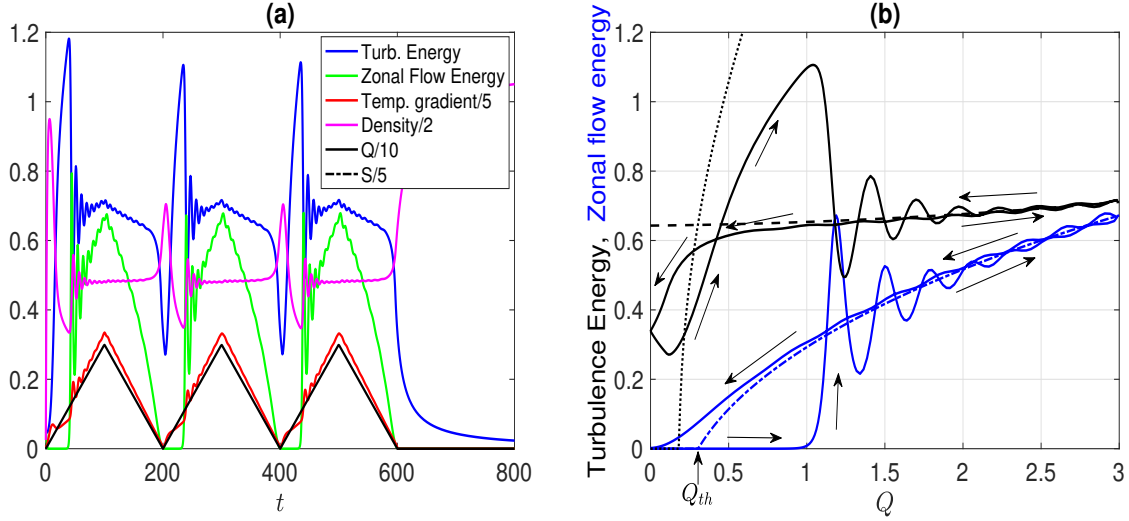


Figure 7. (a): Evolution of turbulence energy, zonal flow energy, temperature gradient and density under the action of a cyclic ramp of input power  $Q$ . (b): Zonal collapse hysteresis in a cyclic power ramp. Hysteresis plots made within the time interval  $t = [200, 400]$ . The black dotted curve is static bifurcation curve for turbulence energy without zonal flow, the black dashed curve is that with zonal flow. The blue dashed dotted curve is the static bifurcation curve for zonal flow energy. The arrows indicate the causal flow of the system.

### 1. Effect of ramp speed $\dot{Q}$ on bifurcation delay

Passage through the bifurcation point ( $Q_{th}$ ) exhibits a delay that depends on the rate of change of the input power  $\dot{Q}$ . This is shown on the left panel of figure(8). We arbitrarily defined the delay as  $Q_j - Q_{th}$ , where  $Q_j$  is the value of  $Q$  when  $\mathcal{E}_z = 0.02$ . The right panel of figure(8) represents this delay as a function of the rate of change  $\dot{Q}$ . We note two distinct regimes. For low values of  $\dot{Q}$ , the delay seems independent of the rate of change. For higher values of  $\dot{Q}$ , the delay follows a power law with the exponent 0.6871.

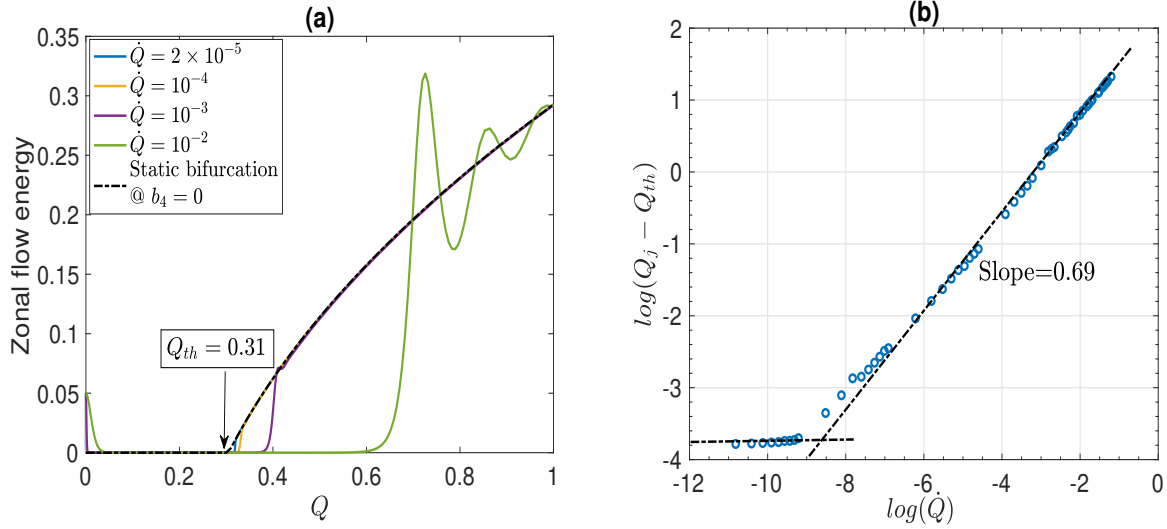


Figure 8. (a): Bifurcation transitions at different ramp rates  $\dot{Q}$ . (b): Bifurcation delay vs. ramp speed. The delay is constant in the limit  $\dot{Q} \rightarrow 0$  and follows a power law  $\dot{Q}^{0.69}$  at finite ramp speeds. Bifurcation delay is defined as the deviation  $Q_j - Q_{th}$ , where  $Q_{th}$  is the steady state threshold power, and  $Q_j$  is the value of  $Q$  when  $\mathcal{E}_z = 0.02$ .

## 2. Hysteresis reduction by zonal noise in cyclic power $Q$ ramp

The effect of zonal noise ( $b_4 \neq 0$ ) on hysteresis loop in a cyclic power ramp is investigated. The results are plotted in figure(9). It can be seen that the degree of hysteresis is reduced with increasing noise parameter. Hysteresis is reduced in all the fields. Notice that the overshoots at the zonal flow excitation are reduced with increasing zonal noise. The zonal noise triggers early transition to the stable branch. As a result, the degree of hysteresis is reduced. However the effect of zonal noise on hysteresis reduction in the  $Q$  ramp is much less than that for in  $S$  ramp. The reason for this is explained later in section(V). This means that the zonal flow hysteresis is more likely to be observed in experiments in a  $Q$  ramp than in a  $S$  ramp.

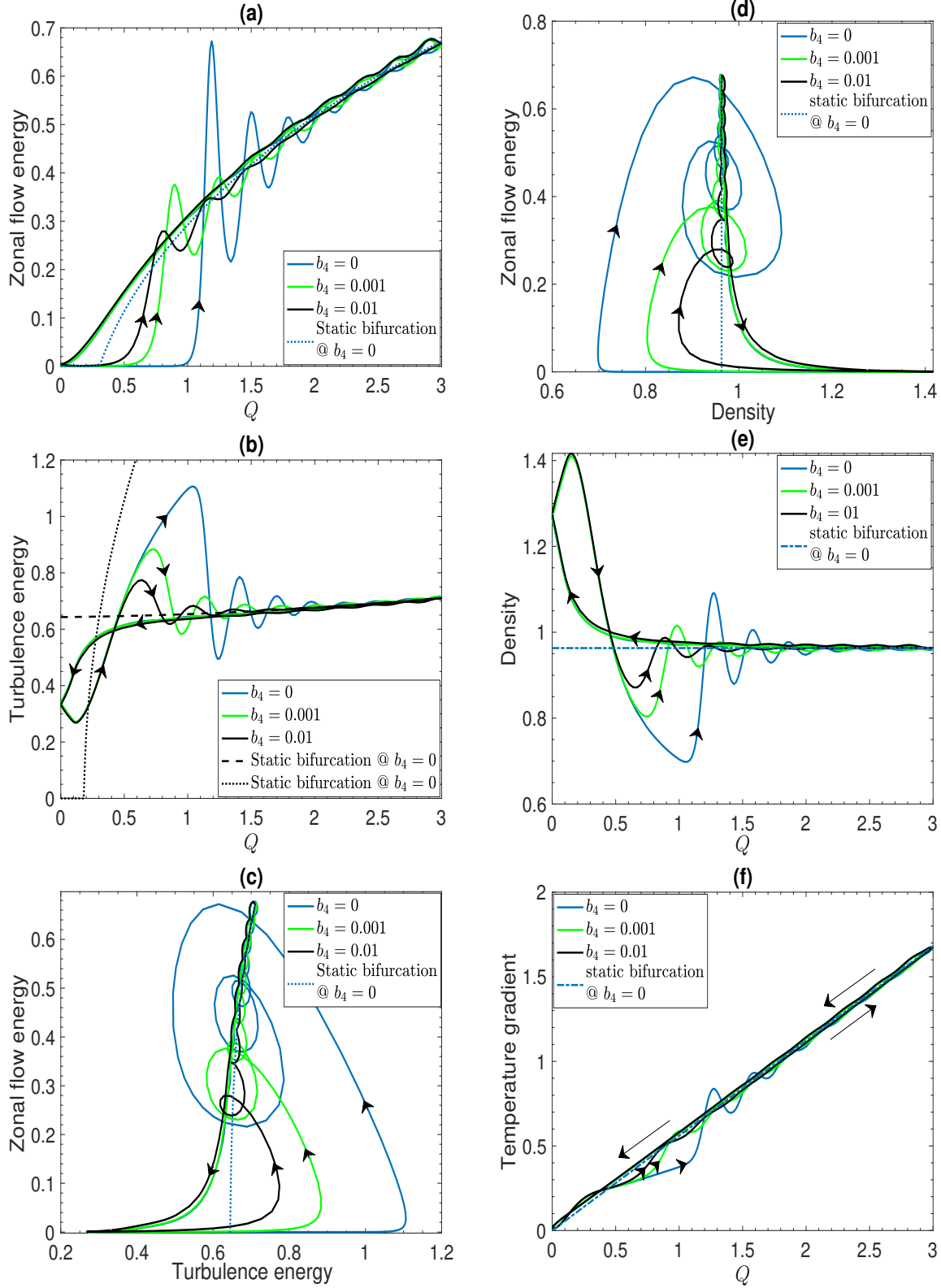


Figure 9. Zonal collapse hysteresis study with a cyclic power  $Q$  ramp. Hysteresis plots made within the time interval  $t = [200, 400]$ . Clearly, noise reduces the degree of hysteresis.

## V. DELAYED BIFURCATION IS THE ORIGIN OF HYSTERESIS

The stability spectra show that the zero zonal flow state is unstable below the bifurcation point. Yet, the system spends significant time in the unstable state before jumping to the finite zonal flow stable state during the  $S$  ramp down? This delayed bifurcation leads to manifestation of hysteresis. So the important question to ask is what is the origin of delayed bifurcation? To understand this, we assume that  $S$  and  $Q$  are ramped adiabatically so that

$$\hat{n}(t) = \frac{S(t)}{d_1(t)\mathcal{E} + d_3} \quad (25)$$

$$\mathcal{T}(t) = \frac{Q(t)}{c_1(t)\mathcal{E} + c_3} \quad (26)$$

This reduces the 4 field model effectively to a 2-field model consisting of  $\mathcal{E}$  and  $\mathcal{E}_z$  with time dependent parameters,

$$\frac{\partial \mathcal{E}}{\partial t} = a_1 \gamma(t) \mathcal{E} - a_2 \mathcal{E}^2 - a_4(t) \mathcal{E}_z \mathcal{E} \quad (27)$$

$$\frac{\partial \mathcal{E}_z}{\partial t} = b_1(t) \mathcal{E} \mathcal{E}_z - b_3 \hat{n}(t) \mathcal{E}_z + b_4 \mathcal{E}^2 \quad (28)$$

where the mean  $E \times B$  shear feedback effects are absorbed in the time parametrized coefficients  $\gamma(t) \equiv \gamma(t)/(1 + b_2 \mathcal{V}^2(t))$ ,  $a_4(t) \equiv a_4/(1 + b_2 \mathcal{V}^2(t))$ ,  $b_1(t) \equiv b_1/(1 + b_2 \mathcal{V}^2(t))$ ,  $c_1(t) \equiv c_1/(1 + b_2 \mathcal{V}^2(t))$  and  $d_1(t) \equiv d_1/(1 + b_2 \mathcal{V}^2(t))$ . Recall that, without the zonal noise i.e.,  $b_4 = 0$ , the critical points are given by

$$\left\{ \begin{array}{l} \mathcal{E} = b_3 \hat{n} / b_1 \\ \mathcal{E}_z = \frac{a_2}{a_4} \left[ \frac{a_1 \gamma}{a_2} - \frac{b_3}{b_1} \hat{n} \right] \end{array} \right\} \quad (29)$$

and

$$\left\{ \begin{array}{l} \mathcal{E} = \frac{a_1 \gamma}{a_2} \\ \mathcal{E}_z = 0 \end{array} \right\}. \quad (30)$$

Around the bifurcation point (both in  $Q$  and  $S$ ), the evolution can be linearized

$$\frac{\partial \mathcal{E}}{\partial t} = -a_1 \gamma(t) \mathcal{E} - a_4(t) \frac{a_1 \gamma(t)}{a_2} \mathcal{E}_z \quad (31)$$

$$\frac{\partial \mathcal{E}_z}{\partial t} = \left( b_1(t) \frac{a_1 \gamma(t)}{a_2} - b_3 \hat{n}(t) \right) \mathcal{E}_z \quad (32)$$

where now  $n(t)$  and  $\gamma(t)$  should be obtained from the coupled nonlinear equations

$$\hat{n}(t) = \frac{S(t)}{d_1(t) \frac{a_1 \gamma(t)}{a_2} + d_3} \quad (33)$$

$$\mathcal{T}(t) = \frac{Q(t)}{c_1(t) \frac{a_1 \gamma(t)}{a_2} + c_3} \quad (34)$$

Once  $n(t)$  and  $\mathcal{T}(t)$  are known in terms of  $S(t)$  and  $Q(t)$ , time-dependent parameters  $b_1(t)$  and  $a_4(t)$  follows directly from mean shear expression given by the radial force balance i.e., equation(5). Turbulence and zonal flow evolutions are described by equations (31) and (32) as long as the solutions  $(\mathcal{E}(t), \mathcal{E}_z(t))$  remain close to the fixed point(30). After a sufficiently long time, the linearization is no longer valid and the solution leaves the neighborhood of the fixed point(30) and diverges exponentially, thus making a transition to the finite zonal flow fixed point(29). After the transition, the equations(31) and (32) no longer describe the dynamics correctly. Assuming that all the time dependent coefficients are known, integration of equation(32) yields

$$\mathcal{E}_z(t) = \mathcal{E}_z(0) \exp \left[ \int_{t_0}^t dt' \left( b_1(t') \frac{a_1 \gamma(t')}{a_2} - b_3 \hat{n}(t') \right) \right] \quad (35)$$

and the integration of equation(31) yields

$$\mathcal{E}(t) = \mathcal{E}(0) e^{-a_1 \int_{t_0}^t dt' \gamma(t')} - \int_{t_0}^t dt'' a_4(t'') \frac{a_1 \gamma(t'')}{a_2} \mathcal{E}_z(t'') e^{-a_1 \int_{t''}^t dt' \gamma(t')} \quad (36)$$

Equation(35) shows that zonal flow energy begins to diverge when the integral  $\int_{t_0}^t dt' \left( b_1(t') \frac{a_1 \gamma(t')}{a_2} - b_3 \hat{n}(t') \right)$  changes sign. This means that the *dynamical bifurcation* occurs at the control parameters  $S(t_*)$  and  $Q(t_*)$  at time  $t_*$  at which the integral  $\int_{t_0}^{t_*} dt' \left( b_1(t') \frac{a_1 \gamma(t')}{a_2} - b_3 \hat{n}(t') \right) = 0$ . The dynamical bifurcation point can differ significantly from the static bifurcation point  $S(\bar{t})$  and  $Q(\bar{t})$  at time  $\bar{t}$  at which  $b_1(\bar{t}) \frac{a_1 \gamma(\bar{t})}{a_2} - b_3 \hat{n}(\bar{t}) = 0$ . For example, for constant  $b_1$  and  $\gamma$  and linearly varying  $\hat{n}$  i.e.,  $\hat{n}(t) = \hat{n}_0 + \epsilon t$ , it is straightforward to see that  $t^* = 2\bar{t}$ . Thus, *bifurcation delay due to time dependent control parameter is at the origin of the hysteresis seen when the control parameter is swept across the static bifurcation point.* Equation(36) show that turbulence energy evolution is slaved by zonal flow near the bifurcation point. Turbulence energy rolls down as the zonal flow energy begins to grow.

Next we analyze the effect of zonal noise on dynamical bifurcation. Linearization of the turbulence energy equation(27) and zonal flow equation(28) with  $b_4 \neq 0$  yields  $\mathcal{E}$  and  $\mathcal{E}_z$  evolution equations with bi-directional coupling with time-dependent coefficients, which is not easy to solve analytically. Hence to make conceptual progress, let us focus on the evolution of the zonal flow and assume that turbulence is in quasi-steady state given by  $\mathcal{E} = \frac{a_1}{a_2} \gamma(t) - \frac{a_4(t)}{a_2} \mathcal{E}_z$ . Substituting this in the zonal flow equation(28) yields

$$\frac{\partial \mathcal{E}_z}{\partial t} = \mathcal{E}_z \left( \left( b_1(t) - 2b_4 \frac{a_4(t)}{a_2} \right) \frac{a_1}{a_2} \gamma(t) - b_3 \hat{n}(t) - \frac{a_4(t)}{a_2} \left( b_1(t) - b_4 \frac{a_4(t)}{a_2} \right) \mathcal{E}_z \right) + b_4 \left( \frac{a_1}{a_2} \gamma(t) \right)^2$$

This equation is clearly in a normal form for transcritical bifurcation with a source term which exist only when  $b_4 \neq 0$ . As long as the system stays close to the zero zonal flow state,

$$\frac{\partial \mathcal{E}_z}{\partial t} = \left( \left( b_1(t) - 2b_4 \frac{a_4(t)}{a_2} \right) \frac{a_1}{a_2} \gamma(t) - b_3 \hat{n}(t) \right) \mathcal{E}_z + b_4 \left( \frac{a_1}{a_2} \gamma(t) \right)^2 \quad (38)$$

The above equation reduces to equation(32) without the zonal noise i.e., when  $b_4 = 0$ . The equation(38) can be integrated to yield

$$\begin{aligned} \mathcal{E}_z(t) = & \mathcal{E}_z(0) \exp \left[ \int_{t_0}^t dt' \left( \left( b_1(t') - 2b_4 \frac{a_4(t')}{a_2} \right) \frac{a_1 \gamma(t')}{a_2} - b_3 \hat{n}(t') \right) \right] \\ & + \int_{t_0}^t dt'' b_4 \left( \frac{a_1}{a_2} \gamma(t'') \right)^2 \exp \left[ \int_{t''}^t dt' \left( \left( b_1(t') - 2b_4 \frac{a_4(t')}{a_2} \right) \frac{a_1 \gamma(t')}{a_2} - b_3 \hat{n}(t') \right) \right] \end{aligned} \quad (39)$$

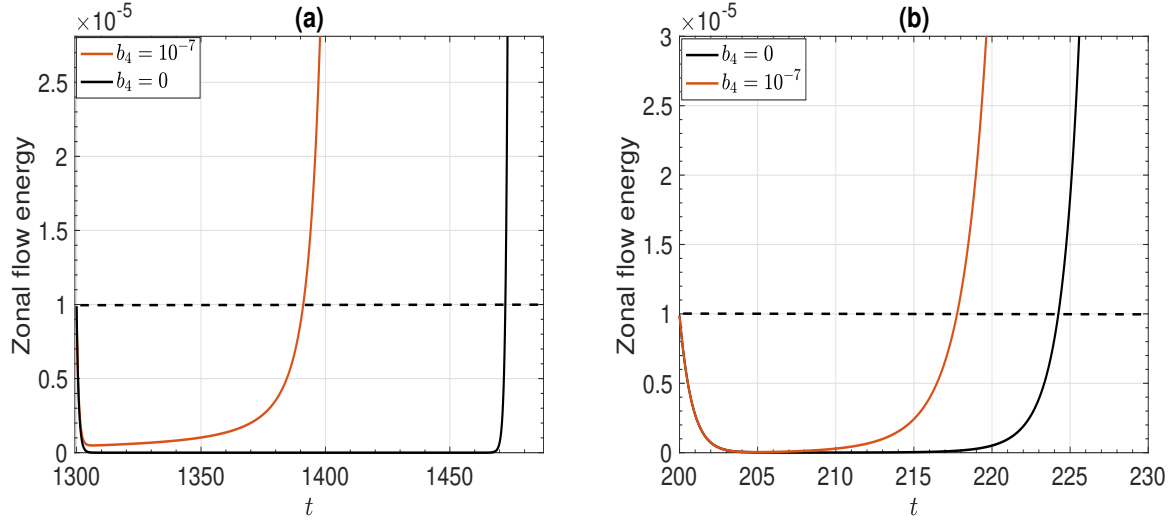


Figure 10. (a): Comparing equations(35) and (39) for initial value of zonal flow  $\mathcal{E}_z(t_0 = 1300) = 10^{-5}$ . The chosen initial time  $t_0 = 1300$  is the time when the particle source  $S$  begins to ramp down in figure(11). (b): Comparing equations(35) and (39) for initial value of zonal flow  $\mathcal{E}_z(t_0 = 200) = 10^{-5}$ . The chosen initial time  $t_0 = 200$  is the time when the heat source  $Q$  begins to ramp up in figure(7)

Comparing equations(35) and (39) show that source term  $b_4 \left( \frac{a_1}{a_2} \gamma(t) \right)^2$  due to zonal noise causes faster growth of zonal flow, than for the case without noise. This is shown in figure(10). Thus, zonal noise knocks the system off the zero zonal flow state and the degree of hysteresis is reduced. The figure also shows that the noise effect is much more drastic for the  $S$  ramp case than for the  $Q$  ramp case. This is a consequence of trade off between zonal flow damping rate and linear growth rate of turbulence. Notice that  $S$  ramp has stronger effect on density variation than  $Q$  ramp. Whereas  $Q$  ramp has stronger effect on the linear growth rate variation than the  $S$  ramp. Below the zonal flow excitation threshold,  $n \sim S$  during  $S$  ramp down whereas  $\gamma \sim Q^{1/3}$  during  $Q$  ramp up. As a result, noise effect appears much more amplified in a  $S$  ramp than in a  $Q$  ramp(see the second term of equation(39)). This explains why the noise kicks the system off the zero zonal flow state much more quickly for the  $S$  ramp case than for the  $Q$  ramp case. As a result, for the same noise parameter, the hysteresis area is much more severely reduced in the  $S$  ramp case than in the  $Q$  ramp case.

In this section, we showed that delayed bifurcation is at the origin of hysteresis. The delay

in the bifurcation is due to critical slowing down at a bifurcation point. The slowing down is due to the fact that the real part of the characteristic eigenvalue tends to vanish near the bifurcation point. As a result the relaxation time increases in the vicinity of the bifurcation point and diverges to infinity at the bifurcation point. Thus, the dynamical bifurcation occurs beyond the static bifurcation point on sweeping the control parameter. The zonal noise knocks the system off the zero zonal flow state much more quickly for the  $S$  ramp case than for the  $Q$  ramp case. Consequently, the degree of hysteresis is much more severely reduced in the  $S$  ramp case than in the  $Q$  ramp case. Hence, zonal collapse hysteresis may not be observed in a S-ramp experiment. Rather, experiments should focus on the zonal flow collapse hysteresis detection in  $Q$  ramp. Though the discussion here is focused on zonal flow collapse bifurcation, the critical slowing down is an universal phenomenon. One wonders what might be the effect of critical slowing down induced bifurcation delay on hysteresis linked with bistability, such as the familiar L-H transition hysteresis? It is not hard to imagine that the bifurcation delay due to the *unavoidable* critical slowing effect will cause “swelling” of the hysteresis loop. As a result, the area of the *dynamical* L-H hysteresis loop should be larger than the static L-H hysteresis loop.

## VI. DISCUSSION AND CONCLUSIONS

Several experiments[34–38], including a recent JET experiment[39], have reported a power ( $Q$ ) scaling of the L mode density limit  $n_{crit} \sim Q^{0.25-0.56}$ . This in contradiction to the power-independent, pure Greenwald density limit[13, 33]. While any radiative collapse density is obviously  $Q$  dependent[41, 63], several experiments now indicate that radiative cooling is secondary to transport bifurcation -in particular a back transition or collapse of the edge shear layer[15]. Hence, a transport based theory is needed to provide deeper insight into the density limit phenomenology. Recent theories[25, 45] linked onset of density limit phenomenology to zonal shear layer collapse. Such a collapse will result in enhanced edge cooling, which can trigger radiative phenomena. Neoclassical zonal flow screening is identified as the key to emergence of the plasma current ( $I_p$ ) scaling of the density limit[45].

But the issue of emergence of power scaling of density limit from the microscopic transport physics remained unaddressed. To this end, in this paper, zonal shear collapse is studied within the framework of a physics based simple 0D model. The model evolves turbulence energy, zonal flow energy, temperature gradient and local density in time. The model includes the neoclassical screening of zonal flow response and stochastic magnetic field effects. Note that magnetic fusion devices often have stochastic magnetic fields in the edge region due to overlapping of magnetic islands localized at the resonant surfaces. The magnetic islands can appear due to breaking of nested toroidal flux surfaces either due to an externally applied resonant magnetic perturbation[46] or due to pressure gradient induced magnetic perturbations in high beta equilibrium[64]. Hence the model yields power, as well as stochastic magnetic field scalings of the density limit. The results are obtained for ITG turbulence but the structure is general- applicable to any turbulence model. The main results are:

1. Analytical static bifurcation analysis, ignoring the mean shear feedback, shows that the critical density  $n_{crit}$  for zonal shear collapse scales with plasma current  $I_p$ , input power  $Q$  and the normalized stochastic field amplitude  $b_{st}^2 (= q \left( \frac{\delta B_r}{B} \right)^2 / \sqrt{\beta} \rho_*^2 \epsilon)$  as

$$n_{crit} \sim \frac{I_p^2 Q^{1/3}}{(1 + b_{st}^2)^{5/3}}$$

Numerical initial value study of zonal shear collapse in a particle source ramp up yields power and stochastic field scalings of critical density consistent with the above theoretical estimate. However, the absolute value of  $n_{crit}$  obtained in source ramp up is higher than  $n_{crit}$  obtained from the static bifurcation analysis. This is because of critical slowing down at the static bifurcation point. *The favorable  $Q$  scaling of the density limit emerges from the fact that the shear layer strength increases with  $Q$ , thus preventing shear layer collapse.* This in turn reduces particle transport and improves particle confinement. Unfavorable  $b_{st}^2$  scaling emerges from the fact that the stochastic fields erode the shear layer[47] by dephasing the Reynolds stress[48]. As a result the particle transport increases and particle confinement degrades. Thus,

ambient stochastic fields accelerate shear layer collapse when density is increased. The favorable current scaling emerges from the fact that the shear layer strength increases with the reduction of neoclassical zonal flow screening on increasing the plasma current  $I_p$ . However, the current scaling here is stronger than Greenwald scaling.

2. All fields (Turbulence energy, zonal flow energy, temperature gradient and density) exhibit hysteresis in  $Q$ , upon cyclic power ramps across the bifurcation point. The hysteresis is due to delayed bifurcation due to critical slowing down. This is fundamentally different from static hysteresis, often associated with bi-stability. The delayed bifurcation manifests as metastability due to a small but finite life time of the zero zonal flow state below the bifurcation point. The bifurcation delay spectra in the power ramp speed  $\dot{Q}$  exhibits two distinct regimes. The delay in bifurcation is independent of  $\dot{Q}$  at small  $\dot{Q}$  and follows a power law  $\dot{Q}^{0.7}$  at higher  $\dot{Q}$  values.
3. All fields also exhibit hysteresis in a cyclic source  $S$  ramp. This is again due to the reasons as explained in the above item 2. The bifurcation delay spectra in the source ramp speed  $\dot{S}$  also exhibits two distinct regimes. The delay in bifurcation is independent of  $\dot{S}$  at small  $\dot{S}$  and follows a power law  $\dot{S}^1$  at higher  $\dot{S}$  values.
4. The zonal noise (incoherent zonal flow emissions) has a dramatic effect on the hysteresis of all fields in the  $S$ -ramp. Even weak zonal noise (much weaker than the phase coherent emission) can kick the system out of the metastable state so quickly that hysteresis disappears. Hence experimental detection of zonal shear collapse hysteresis in  $S$  is likely to be very difficult. On the other hand, the zonal noise reduces the degree of hysteresis in the  $Q$ -ramp much less dramatically than in the  $S$ -ramp. Hence, the hysteresis should be more easily observed in  $Q$  ramp than in  $S$  ramp. Reduction of zonal flow damping ( $\gamma_d \sim n \sim S$ ) during  $S$  ramp down is stronger than linear growth rate ( $\gamma \sim Q^{1/3}$ ) increase during  $Q$  ramp up. As a result the effect of zonal noise appears much more amplified in a  $S$  ramp than in a  $Q$  ramp (see equation(39) and figure(10)).

One might wonder that many theoretical studies in the past have demonstrated  $Q$  dependence of the density limit. Then what is new here? Well, all previous theoretical studies demonstrating power dependence of the density limit were all based on the radiative collapse paradigm. It is not at all surprising to get a power dependence from radiative models because increasing the power decreases the radiation. This simplistic macroscopic power balance approach does not address the detailed microscopic dynamics responsible for triggering of cooling events and the subsequent emergence of density limit phenomenology. We presented the *first* microscopic transport physics based model of the emergence of power scaling of the density limit. This is based on the shear layer collapse paradigm. Transport bifurcation accompanied by shear layer collapse reduces temperature. This then causes local edge cooling, which can enhance radiation thus triggering a radiative cooling event, e.g., radiative condensation or MARFEs. Increasing the power increases the shear layer strength. The enhanced turbulence decorrelation by zonal shear reduces the outward particle flux. As a result the particle confinement improves, thus increasing the density limit.

All the analysis presented in this paper is valid strictly for the L (low confinement) mode density limit. The H (high confinement) mode density limit is also expected to exhibit a power dependence. While the L mode density limit is connected with the zonal shear layer collapse, the H mode density limit is related to mean ExB shear collapse. The zero zonal flow state can be thought as the density limit (DL) state. The H mode density limit is linked to the back transition of the system from the H mode to the L mode. Note that zonal flows are absent in H mode. In this case mean ExB shear layer collapse tracks the H→L back transition. Mean shear layer strength also increases with the input power. Hence, the H mode density limit should also exhibit a power scaling, as shown in Refs[65, 66]. However, H mode density limit power scaling need not necessarily be same as the L mode density limit power scaling. It was observed on both machines JET and ASDEX that detachment, as well as the X-point MARFE itself, does not trigger a transition in the confinement regime and thus does not present a limit on the plasma density. The understanding of mean shear collapse at high density is still elusive. Heuristic arguments based on MHD ballooning stability of SOL[67, 68] fail to provide an understanding of mean ExB shear collapse at high

density. Recently, collisional broadening of SOL has been proposed as a mechanism of SOL shear layer collapse, which can induce an H→L back transition[69]. The physics of mean shear ExB shear collapse at high density and possible power scaling of H mode density limit will be subjects of future research.

Zonal flows regulate turbulence before the transition to the H mode. They trigger the transition by lowering the power threshold, relative to the case when zonal flows are absent. Thus, zonal flows accelerate the L→H transition for fixed power ramp and disappear after the transition. L→DL transition is also marked by disappearance of zonal flows i.e., zonal flow shear collapse. Here, the zonal shear collapse is induced when the zonal flow damping exceeds the drive during the source ramp up. During the L→DL back transition, the zonal flow energy is depleted and the internal energy of fluctuations increases. In contrast, the zonal flow energy depletion during the L→H transition is accompanied by depletion of turbulence energy. This is because of steep rise in the mean ExB shear which kills the turbulence.

Like L→H transition the L→DL (or finite zonal flow to zero zonal flow) transition in also hysteretic. The hysteresis is symptomatic of a transport bifurcation process. However the origin of L-DL hysteresis is fundamentally different from the L-H hysteresis. The L-H hysteresis is due to the transition between the two stable states, L and H. In the case of L-H hysteresis, dynamical effects (i.e, finite rate  $\dot{Q}$ ) increases the area of the hysteresis loop compared to the static bifurcation hysteresis loop. The L-DL hysteresis is solely due to the delay in bifurcation transition between the static stable and unstable states when the power is swept across the static bifurcation point. Delay in bifurcation manifests as dynamic metastability of the unstable zero zonal flow state below the static bifurcation point. Experimental observation of L-H hysteresis confirms that the L→H transition is a transport bifurcation process. Thus hysteresis can be used as probe to study transport bifurcation. Similarly experimental detection of L-DL hysteresis would confirm that the L→DL (DL→L) transition is a manifestation of transport bifurcation process primarily associated with zonal shear layer death (birth).

Finally, our conclusions are also valid for the density limit phenomenology in stellarators.

This follows from the fact that the model developed here links density limit to the edge shear layer, which is present in all known devices. The edge shear layer is controlled by the zonal flow screening response, collisional damping and input power. A recent experiment on TJ-II stellarator[70] shows edge cooling, decline in stored energy and long range correlations (LRC) at densities close to the density limit. This is qualitatively consistent with our analysis and conclusions. It is also shown that the critical density for LRC collapse increases with increasing NBI power. This is again qualitatively consistent with our conclusions. This is simply because the zonal flow strength increases with input power, which prevents the shear layer collapse. This in turn improves particle confinement and increases the density limit. Notice that our model yields power scaling of  $\sim Q^{1/3}$ , which is slightly weaker than the Sudo's empirical scaling of  $\sim Q^{1/2}$ [71]. While this is encouraging, a power scan of LRC collapse density is desirable to make a direct comparison of power scaling with our model results.

### ACKNOWLEDGMENTS

The authors thank discussions with A. Garofalo, M. Greenwald, R. Hong, G. Tynan, Z. Yan, C. Holland, L. Schmitz and T. Long. This research was supported by U.S. DOE under Award No. *DE – FG02 – 04ER54738*.

### Appendix A: Zonal shear collapse hysteresis with cyclic source $S$ ramp

The results without the zonal noise are plotted in figure(11). Left panel of figure(11) shows the time evolution of turbulence energy, zonal flow energy, temperature gradient, density when the particle source is ramped periodically. Following are the striking features of this plot:

- Turbulence, zonal flow energy, temperature gradient and density - all has broken time - symmetry with respect to the maximum of the source function. This means all fields exhibit hysteresis.

- Zonal flow decay in the  $S$  ramp up phase is much slower than the zonal flow growth in the  $S$  ramp down phase.

Right panel of figure(11) show hysteresis plot of zonal flow and turbulence energy in  $S$  with the static bifurcation curves (in red dashed and dashed-dotted) superposed. The two static bifurcation curves correspond to the roots

$$\left\{ \begin{array}{l} \mathcal{E} = b_3 \hat{n} (1 + b_2 \mathcal{V}^2) / b_1 \\ \mathcal{E}_z = \frac{a_2}{a_4} (1 + b_2 \mathcal{V}^2) \left[ \frac{a_1}{a_2} \frac{\gamma}{(1 + b_2 \mathcal{V}^2)} - \frac{b_3}{b_1} \hat{n} (1 + b_2 \mathcal{V}^2) \right] \\ \mathcal{T} = \frac{Q}{c_1 \frac{\mathcal{E}}{1 + c_2 \mathcal{V}^2} + c_3} \\ \hat{n} = \frac{S}{d_1 \frac{\mathcal{E}}{1 + d_2 \mathcal{V}^2} + d_3} \end{array} \right\} \quad (\text{A1})$$

and

$$\left\{ \begin{array}{l} \mathcal{E} = \frac{a_1}{a_2} \frac{\gamma}{1 + a_3 \mathcal{V}^2} \\ \mathcal{E}_z = 0 \\ \mathcal{T} = \frac{Q}{c_1 \frac{\mathcal{E}}{1 + c_2 \mathcal{V}^2} + c_3} \\ \hat{n} = \frac{S}{d_1 \frac{\mathcal{E}}{1 + d_2 \mathcal{V}^2} + d_3} \end{array} \right\}. \quad (\text{A2})$$

Clearly, the hysteresis appears due to delayed jumping of the solution between these two steady states. This is evident from the hysteresis plot shown on right panel of figure(11) where the static bifurcation curves are superposed for clarity. The stability of the fixed points are analyzed next.

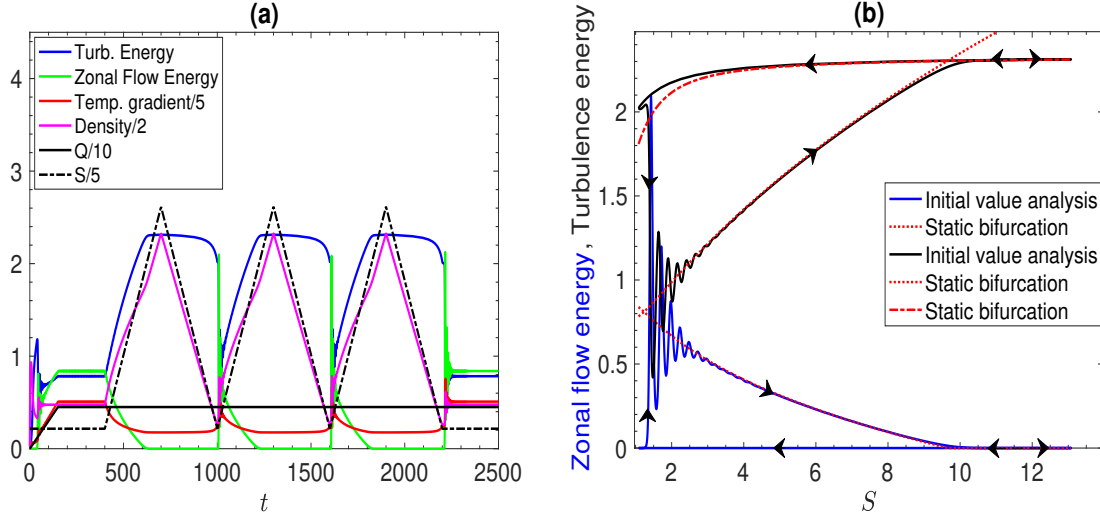


Figure 11. (a): Temporal evolution of the system under the action of a cyclic particle source  $S$  ramp. (b): Zonal flow and turbulence hysteresis in  $S$ . Hysteresis plots made within the time interval  $t = [1000, 1600]$ .

*a. Stability spectra of the fixed points in a source  $S$  ramp*

The stability of the fixed points are determined by the eigenvalues of the Jacobian at the fixed points. The  $S$ - spectra of the eigenvalues of the Jacobian of the system of equations(1), (2), (3), (4) and (5) are calculated. The left panel of Figure(12) show eigenvalues of the finite zonal flow branch given by equation(A1). The right panel of Figure(12) show eigenvalues of the zero zonal flow branch corresponding to equation(A2). All the real parts of the eigenvalues of the finite zonal flow branch are negative. Clearly, the finite zonal flow branch is stable. On the other hand the zero zonal flow branch has at least one eigenvalue with positive real part. This means that the zero zonal flow branch is unstable or metastable. Notice that the imaginary parts of the eigenvalues of the stable branch are larger, and spans over a wider range in  $S$ , than those for the unstable branch. This explains why the system is more oscillatory in the beginning of the  $S$  ramp up phase than that in the  $S$  ramp down phase. The cross-over point ( $S = 9.6$ ) of the stable and the unstable branch is the static bifurcation point where the two branches exchange their stability.

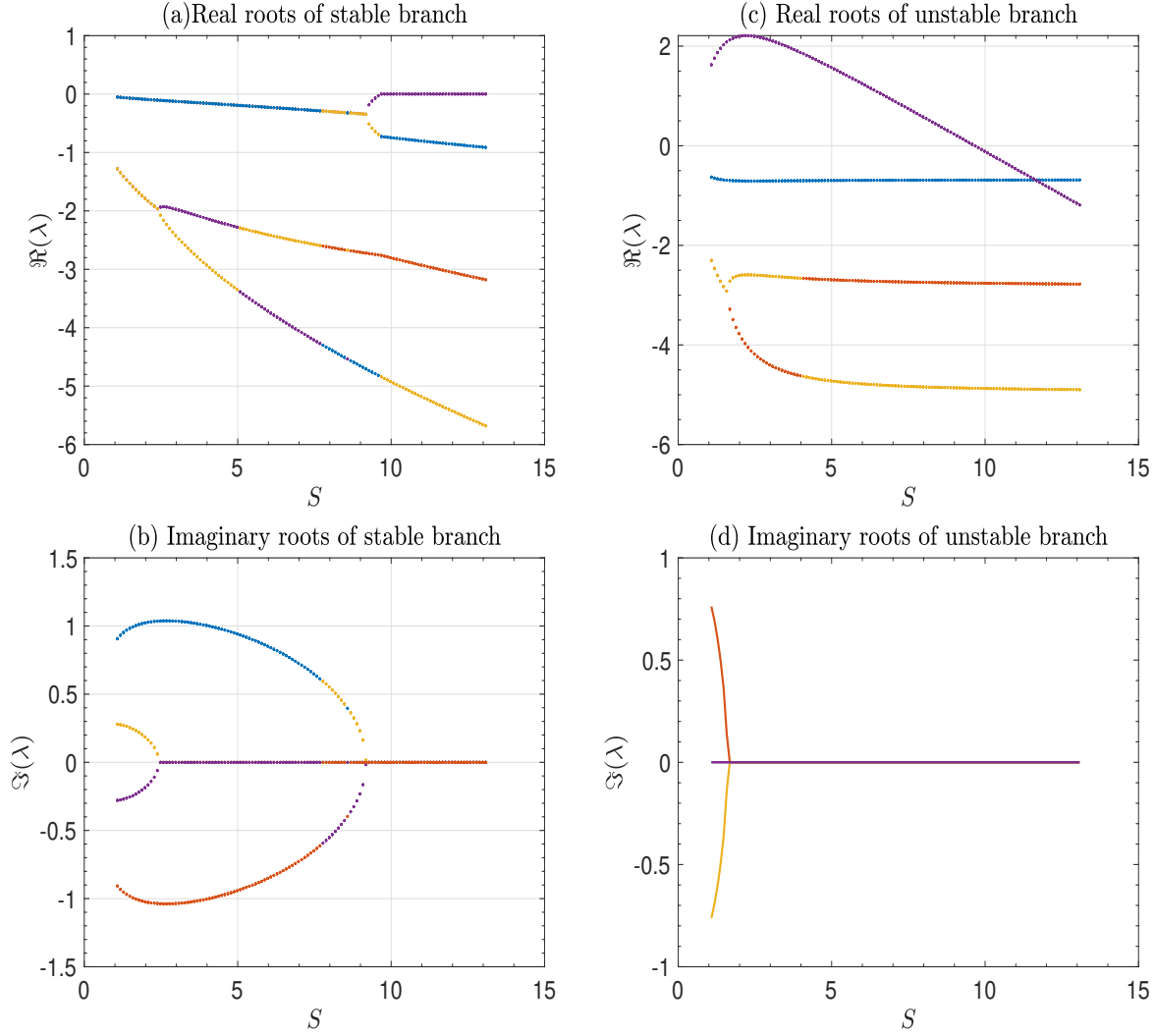


Figure 12. (a): Real part of the eigenvalues of the stable branch (corresponding to the lower turbulence energy and finite zonal flow energy branch). (b): Imaginary part of the eigenvalues of the stable branch. (c): Real part of the eigenvalues of the unstable branch (corresponding to the higher turbulence energy and zero zonal flow energy branch). (d): Imaginary part of the eigenvalues of the unstable branch. The state with finite zonal flow and low turbulence is stable while the state with zero zonal flow and high turbulence is unstable. Cross-over of these two states in  $S$  space yields the bifurcation point. This is generic of transcritical bifurcation where two fixed point branches exchange stability at the bifurcation point. Zero zonal flow state is unstable below the bifurcation point and stable above it. While the finite zonal flow state is stable below the bifurcation point and unstable above it.

*b. Effect of source ramp speed  $\dot{S}$  on bifurcation delay*

Passage through the steady state bifurcation point ( $S_{crit}$ ) exhibits a delay that depends on the rate of change of the particle source  $\dot{S}$ . This is shown on the left panel of figure(13).

We arbitrarily defined the delay as  $S_j - S_{crit}$ , where  $S_j$  is the value of  $S$  when  $\mathcal{E}_z = 10^{-5}$ . The right panel of figure(13) represents this delay as a function of the rate of change  $\dot{S}$ . We note two distinct regimes. For low values of  $\dot{S}$ , the delay seems independent of the rate of change. For higher values of  $\dot{S}$ , the delay follows a power law with the exponent 0.98.

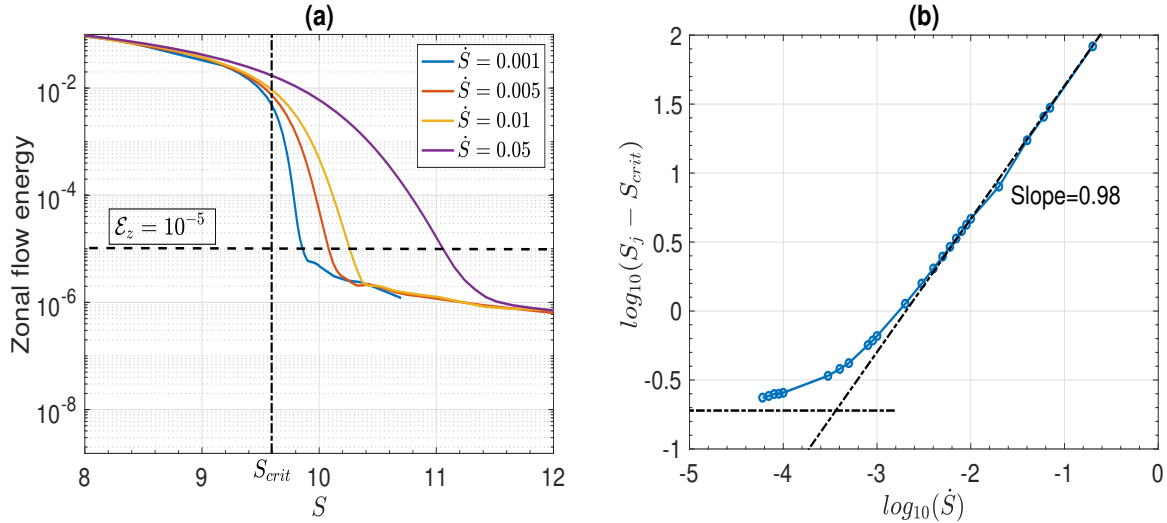


Figure 13. (a): Bifurcation transitions at different ramp speeds  $\dot{S}$ . (b): Bifurcation delay vs. ramp speed. The delay is constant in the limit  $\dot{S} \rightarrow 0$  and follows a power law  $\dot{S}^{0.98}$  at finite ramp speeds. Bifurcation delay is defined as the deviation  $S_j - S_{crit}$ , where  $S_{crit}$  is the steady state critical particle source, and  $S_j$  is the value of  $S$  when  $\mathcal{E}_z = 10^{-5}$ .

*c. Hysteresis reduction by zonal noise in cyclic source  $S$  ramp*

Next, we investigated the effect of zonal noise ( $b_4 \neq 0$ ) on hysteresis loop in a cyclic source ramp. The results are plotted in figure(14). It can be seen that the hysteresis is drastically reduced, even by a very weak zonal noise of the order of  $b_4 = 10^{-8}, 10^{-7}$ . Hysteresis is reduced in all the fields. The overshoots at the time of zonal flow excitation are also reduced drastically. With noise, the system closely follows the stable branch during  $S$  ramp up. However, it is quickly knocked off the unstable branch during the  $S$  ramp down phase. In other words a small zonal noise triggers an early transition to the stable branch. This is explained further later in section(V). As a result the degree of hysteresis is drastically reduced. For higher values of zonal noise parameter, comparable to modulational growth parameter in magnitude, the hysteresis disappears from all fields. The system simply retreats

on to the same path. This happens because, at finite zonal noise, the static bifurcation point is lost from the range of variation of  $S$ . Hence zonal flow hysteresis may not be easily observed in  $S$  ramp.

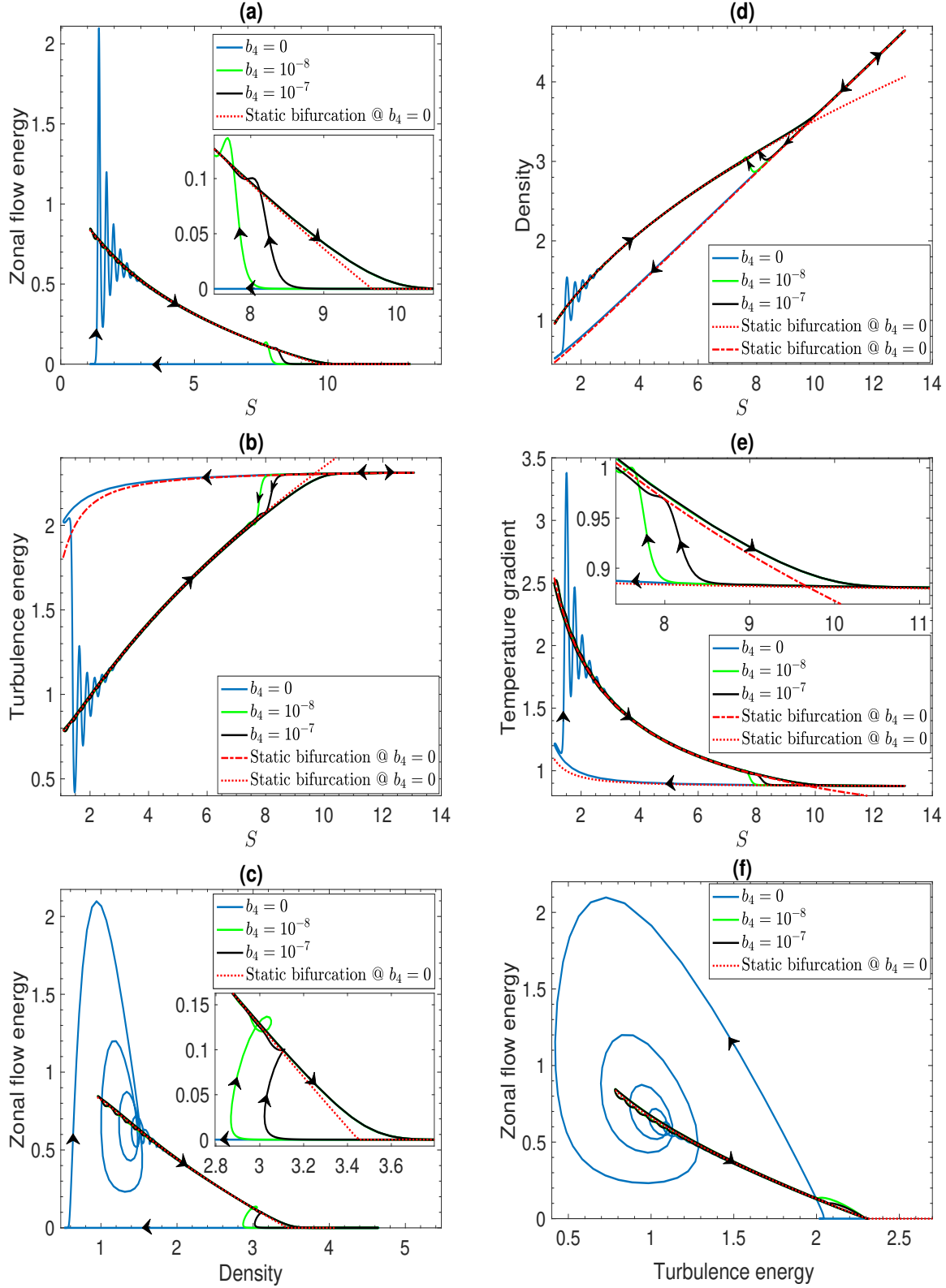


Figure 14. (a): Zonal flow energy hysteresis in  $S$ . (b): Turbulence energy hysteresis in  $S$ . (c): Zonal flow energy hysteresis in  $n$ . (d): Density hysteresis in  $S$ . (e): Temperature gradient hysteresis in  $S$ . (f): Turbulence energy and Zonal flow energy phase plane. Notice, drastic reduction in the degree of hysteresis by noise. The figure insets show zoom in near the bifurcation point. Plots made within the time interval  $t = [1000, 1600]$ .

- 
- [1] F. Wagner, G. Becker, K. Behringer, D. Campbell, A. Eberhagen, W. Engelhardt, G. Fussmann, O. Gehre, J. Gernhardt, G. v. Gierke, G. Haas, M. Huang, F. Karger, M. Keilhacker, O. Klüber, M. Kornherr, K. Lackner, G. Lisitano, G. G. Lister, H. M. Mayer, D. Meisel, E. R. Müller, H. Murmann, H. Niedermeyer, W. Poschenrieder, H. Rapp, H. Röhr, F. Schneider, G. Siller, E. Speth, A. Stäbler, K. H. Steuer, G. Venus, O. Vollmer, and Z. Yü, *Phys. Rev. Lett.* **49**, 1408 (1982).
- [2] F. Wagner, *Plasma Physics and Controlled Fusion* **49**, B1 (2007).
- [3] S. Kaye, M. Bell, K. Bol, D. Boyd, K. Brau, D. Buchenauer, R. Budny, A. Cavallo, P. Couture, T. Crowley, D. Darrow, H. Eubank, R. Fonck, R. Goldston, B. Grek, K. Jaehnig, D. Johnson, R. Kaita, H. Kugel, B. Leblanc, J. Manickam, D. Manos, D. Mansfield, E. Mazzucato, R. McCann, D. McCune, K. McGuire, D. Mueller, A. Murdock, M. Okabayashi, K. Okano, D. Owens, D. Post, M. Reusch, G. Schmidt, S. Sesnic, R. Slusher, S. Suckewer, C. Surko, H. Takahashi, F. Tenney, H. Towner, and J. Valley, *Journal of Nuclear Materials* **121**, 115 (1984).
- [4] V. Erckmann, F. Wagner, J. Baldzuhn, R. Brakel, R. Burhenn, U. Gasparino, P. Grigull, H. J. Hartfuss, J. V. Hofmann, R. Jaenicke, H. Niedermeyer, W. Ohlendorf, A. Rudyj, A. Weller, S. D. Bogdanov, B. Bombarda, A. A. Borschevsky, G. Cattanei, A. Dodhy, D. Dorst, A. Elsner, M. Endler, T. Geist, L. Giannone, H. Hacker, O. Heinrich, G. Herre, D. Hildebrandt, V. I. Hiznyak, V. I. Il'in, W. Kasperek, F. Karger, M. Kick, S. Kubo, A. N. Kuftin, V. I. Kurbatov, A. Lazaros, S. A. Malygin, V. I. Malygin, K. McCormick, G. A. Müller, V. B. Orlov, P. Pech, I. N. Roi, F. Sardei, S. Sattler, F. Schneider, U. Schneider, P. G. Schüller, G. Siller, U. Stroth, M. Tutter, E. Unger, H. Wolff, E. Würsching, and S. Zöpfel, *Phys. Rev. Lett.* **70**, 2086 (1993).
- [5] R. J. Taylor, M. L. Brown, B. D. Fried, H. Grote, J. R. Liberati, G. J. Morales, P. Pribyl, D. Darrow, and M. Ono, *Phys. Rev. Lett.* **63**, 2365 (1989).
- [6] G. D. Conway, C. Angioni, F. Ryter, P. Sauter, and J. Vicente (ASDEX Upgrade Team), *Phys. Rev. Lett.* **106**, 065001 (2011).

- [7] L. Schmitz, L. Zeng, T. L. Rhodes, J. C. Hillesheim, E. J. Doyle, R. J. Groebner, W. A. Peebles, K. H. Burrell, and G. Wang, *Phys. Rev. Lett.* **108**, 155002 (2012).
- [8] K. H. Burrell, K. Barada, X. Chen, A. M. Garofalo, R. J. Groebner, C. M. Muscatello, T. H. Osborne, C. C. Petty, T. L. Rhodes, P. B. Snyder, W. M. Solomon, Z. Yan, and L. Zeng, *Physics of Plasmas* **23**, 056103 (2016), <https://doi.org/10.1063/1.4943521>.
- [9] H. Biglari, P. H. Diamond, and P. W. Terry, *Physics of Fluids B: Plasma Physics* **2**, 1 (1990), <https://doi.org/10.1063/1.859529>.
- [10] P. H. Diamond, Y.-M. Liang, B. A. Carreras, and P. W. Terry, *Phys. Rev. Lett.* **72**, 2565 (1994).
- [11] P. H. Diamond, S.-I. Itoh, K. Itoh, and T. S. Hahm, *Plasma. Phys. Cont* **47**, R35 (2005).
- [12] B. N. Rogers, J. F. Drake, and A. Zeiler, *Phys. Rev. Lett.* **81**, 4396 (1998).
- [13] M. Greenwald, *Plasma Physics and Controlled Fusion* **44**, R27 (2002).
- [14] M. Greenwald, A. Bader, S. Baek, M. Bakhtiari, H. Barnard, W. Beck, W. Bergerson, I. Bespamyatnov, P. Bonoli, D. Brower, D. Brunner, W. Burke, J. Candy, M. Churchill, I. Cziegler, A. Diallo, A. Dominguez, B. Duval, E. Edlund, P. Ennever, D. Ernst, I. Faust, C. Fiore, T. Fredian, O. Garcia, C. Gao, J. Goetz, T. Golfinopoulos, R. Granetz, O. Grulke, Z. Hartwig, S. Horne, N. Howard, A. Hubbard, J. Hughes, I. Hutchinson, J. Irby, V. Izzo, C. Kessel, B. LaBombard, C. Lau, C. Li, Y. Lin, B. Lipschultz, A. Loarte, E. Marmor, A. Mazurenko, G. McCracken, R. McDermott, O. Meneghini, D. Mikkelsen, D. Mossessian, R. Mumgaard, J. Myra, E. Nelson-Melby, R. Ochoukov, G. Olynyk, R. Parker, S. Pitcher, Y. Podpaly, M. Porkolab, M. Reinke, J. Rice, W. Rowan, A. Schmidt, S. Scott, S. Shiraiwa, J. Sierchio, N. Smick, J. A. Snipes, P. Snyder, B. Sorbom, J. Stillerman, C. Sung, Y. Takase, V. Tang, J. Terry, D. Terry, C. Theiler, A. Tronchin-James, N. Tsujii, R. Vieira, J. Walk, G. Wallace, A. White, D. Whyte, J. Wilson, S. Wolfe, G. Wright, J. Wright, S. Wukitch, and S. Zweben, *Physics of Plasmas* **21**, 110501 (2014), <https://doi.org/10.1063/1.4901920>.
- [15] R. Hong, G. Tynan, P. Diamond, L. Nie, D. Guo, T. Long, R. Ke, Y. Wu, B. Yuan, and M. X. and, *Nuclear Fusion* **58**, 016041 (2017).

- [16] T. Long, P. Diamond, R. Ke, L. Nie, M. Xu, X. Zhang, B. Li, Z. Chen, X. Xu, Z. Wang, T. Wu, W. Tian, J. Yuan, B. Yuan, S. Gong, C. Xiao, J. Gao, Z. Hao, N. Wang, Z. Chen, Z. Yang, L. Gao, Y. Ding, Y. Pan, W. Chen, G. Hao, J. Li, W. Zhong, and X. Duan, *Nuclear Fusion* **61**, 126066 (2021).
- [17] J. F. Drake, *The Physics of Fluids* **30**, 2429 (1987), <https://aip.scitation.org/doi/pdf/10.1063/1.866133>.
- [18] P. H. Rebut and M. Hugon., *Plasma Physics and Controlled Nuclear Fusion Research, Tenth Conference Proceedings, London, 12-19 September 1984* **2**, 197 (1985).
- [19] D. A. Gates, D. P. Brennan, L. Delgado-Aparicio, Q. Teng, and R. B. White, *Physics of Plasmas* **23**, 056113 (2016), <https://doi.org/10.1063/1.4948624>.
- [20] D. A. Gates and L. Delgado-Aparicio, *Phys. Rev. Lett.* **108**, 165004 (2012).
- [21] C. P. Ritz, H. Lin, T. L. Rhodes, and A. J. Wootton, *Phys. Rev. Lett.* **65**, 2543 (1990).
- [22] Y. Xu, D. Carralero, C. Hidalgo, S. Jachmich, P. Manz, E. Martines, B. van Milligen, M. Pedrosa, M. Ramisch, I. Shesterikov, C. Silva, M. Spolaore, U. Stroth, and N. Vianello, *Nuclear Fusion* **51**, 063020 (2011).
- [23] B. Schmid, P. Manz, M. Ramisch, and U. Stroth, *Phys. Rev. Lett.* **118**, 055001 (2017).
- [24] T. S. Hahm and P. H. Diamond, *J. Kor. Phys. Soc.* **73**, 747 (2018).
- [25] R. J. Hajjar, P. H. Diamond, and M. A. Malkov, *Physics of Plasmas* **25**, 062306 (2018), <https://doi.org/10.1063/1.5030345>.
- [26] S. J. Camargo, D. Biskamp, and B. D. Scott, *Phys. Plasmas* **2**, 48 (1995).
- [27] X. Q. Xu, W. M. Nevins, T. D. Rognlien, R. H. Bulmer, M. Greenwald, A. Mahdavi, L. D. Pearlstein, and P. Snyder, *Physics of Plasmas* **10**, 1773 (2003), <https://doi.org/10.1063/1.1566032>.
- [28] R. Numata, R. Ball, and R. L. Dewar, *Physics of Plasmas* **14**, 102312 (2007), <https://doi.org/10.1063/1.2796106>.
- [29] A. V. Pushkarev, W. J. T. Bos, and S. V. Nazarenko, *Physics of Plasmas* **20**, 042304 (2013), <https://doi.org/10.1063/1.4802187>.
- [30] K. Ghantous and O. D. Gürcan, *Phys. Rev. E* **92**, 033107 (2015).

- [31] T. Eich, P. Manz, and the ASDEX Upgrade team, *Nuclear Fusion* **61**, 086017 (2021).
- [32] R. Ke, P. H. Diamond, T. Long, M. Xu, Z. Chen, L. Gao, Q. Yang, Y. Wang, X. Zhang, L. Nie, T. Wu, J. Gao, D. Li, N. Wang, Z. Yang, Z. y. Chen, Y. Pan, and X. Duan, *Nuclear Fusion* (2022).
- [33] M. Greenwald, J. Terry, S. Wolfe, S. Ejima, M. Bell, S. Kaye, and G. Neilson, *Nuclear Fusion* **28**, 2199 (1988).
- [34] A. Stabler, K. McCormick, V. Mertens, E. Muller, J. Neuhauser, H. Niedermeyer, K.-H. Steuer, H. Zohm, F. Dollinger, A. Eberhagen, G. Fussmann, O. Gehre, J. Gernhardt, T. Hartinger, J. Hofmann, E. Kakoulidis, M. Kaufmann, G. Kyriakakis, R. Lang, H. Murmann, W. Poschenrieder, F. Ryter, W. Sandmann, U. Schneider, G. Siller, F. Soldner, N. Tsois, O. Vollmer, and F. Wagner, *Nuclear Fusion* **32**, 1557 (1992).
- [35] V. Mertens, M. Kaufmann, J. Neuhauser, J. Schweinzer, J. Stober, K. Buchl, O. Gruber, G. Haas, A. Herrmann, A. Kallenbach, and M. Weinlich, *Nuclear Fusion* **37**, 1607 (1997).
- [36] J. Rapp, P. D. Vries, F. SchÄCeller, M. Tokar', W. Biel, R. Jaspers, H. Koslowski, A. KrÄ€mer-Flecken, A. Kreter, M. Lehnen, A. Pospieszczyk, D. Reiser, U. Samm, and G. Sergienko, *Nuclear Fusion* **39**, 765 (1999).
- [37] G. Duesing, *Plasma Physics and Controlled Fusion* **28**, 1429 (1986).
- [38] Y. Kamada, N. Hosogane, R. Yoshino, T. Hirayama, and T. Tsunematsu, *Nuclear Fusion* **31**, 1827 (1991).
- [39] A. Huber, S. Brezinsek, M. Groth, P. de Vries, V. Riccardo, G. van Rooij, G. Sergienko, G. Arnoux, A. Boboc, P. Bilkova, G. Calabro, M. Clever, J. Coenen, M. Beurskens, T. Eich, S. Jachmich, M. Lehnen, E. Lerche, S. Marsen, G. Matthews, K. McCormick, A. Meigs, P. Mertens, V. Philipps, J. Rapp, U. Samm, M. Stamp, M. Wischmeier, and S. Wiesen, *Journal of Nuclear Materials* **438**, S139 (2013), proceedings of the 20th International Conference on Plasma-Surface Interactions in Controlled Fusion Devices.
- [40] J. W. Connor and S. You, *Plasma Physics and Controlled Fusion* **44**, 121 (2001).
- [41] P. Zanca, F. Sattin, and D. Escande, *Nuclear Fusion* **59**, 126011 (2019).
- [42] E. J. Kim and P. H. Diamond, *Phys. Rev. Lett.* **90**, 185006 (2003).

- [43] F. L. Hinton and J. A. Robertson, *The Physics of Fluids* **27**, 1243 (1984), <https://aip.scitation.org/doi/pdf/10.1063/1.864478>.
- [44] M. N. Rosenbluth and F. L. Hinton, *Phys. Rev. Lett.* **80**, 724 (1998).
- [45] R. Singh and P. Diamond, *Nuclear Fusion* **61**, 076009 (2021).
- [46] T. E. Evans, R. A. Moyer, P. R. Thomas, J. G. Watkins, T. H. Osborne, J. A. Boedo, E. J. Doyle, M. E. Fenstermacher, K. H. Finken, R. J. Groebner, M. Groth, J. H. Harris, R. J. La Haye, C. J. Lasnier, S. Masuzaki, N. Ohyaabu, D. G. Pretty, T. L. Rhodes, H. Reimerdes, D. L. Rudakov, M. J. Schaffer, G. Wang, and L. Zeng, *Phys. Rev. Lett.* **92**, 235003 (2004).
- [47] D. M. Kriete, G. R. McKee, L. Schmitz, D. R. Smith, Z. Yan, L. A. Morton, and R. J. Fonck, *Physics of Plasmas* **27**, 062507 (2020), <https://doi.org/10.1063/1.5145207>.
- [48] C.-C. Chen, P. H. Diamond, R. Singh, and S. M. Tobias, *Physics of Plasmas* **28**, 042301 (2021), <https://doi.org/10.1063/5.0041072>.
- [49] D. M. Thomas, R. J. Groebner, K. H. Burrell, T. H. Osborne, and T. N. Carlstrom, *Plasma Physics and Controlled Fusion* **40**, 707 (1998).
- [50] M. A. Malkov and P. H. Diamond, *Phys. Plasmas* **15** (2008).
- [51] K. Miki, P. Diamond, N. Fedorczak, A. G. Ceran, M. Malkov, C. Lee, Y. Kosuga, G. Tynan, G. Xu, T. Estrada, D. McDonald, L. Schmitz, and K. Zhao, *Nuclear Fusion* **53**, 073044 (2013).
- [52] F. L. Hinton, *Physics of Fluids B: Plasma Physics* **3**, 696 (1991), <https://doi.org/10.1063/1.859866>.
- [53] F. L. Hinton and G. M. Staebler, *Phys. Fluids B* **5**, 1281 (1993).
- [54] R. Singh and P. H. Diamond, *Plasma Physics and Controlled Fusion* **63**, 035015 (2021).
- [55] A. S. Ware, P. W. Terry, B. A. Carreras, and P. H. Diamond, *Physics of Plasmas* **5**, 173 (1998), <https://doi.org/10.1063/1.872685>.
- [56] E.-j. Kim and P. H. Diamond, *Phys. Rev. Lett.* **91**, 075001 (2003).
- [57] P. W. Terry, D. E. Newman, and A. S. Ware, *Phys. Rev. Lett.* **87**, 185001 (2001).
- [58] J. Anderson, H. Nordman, R. Singh, and J. Weiland, *Physics of Plasmas* **9**, 4500 (2002), <https://doi.org/10.1063/1.1510450>.

- [59] R. Singh, R. Singh, P. Kaw, O. D. Gurcan, and P. H. Diamond, *Physics of Plasmas* **21**, 102306 (2014), <https://doi.org/10.1063/1.4898207>.
- [60] A. M. Dimits, G. Bateman, M. A. Beer, B. I. Cohen, W. Dorland, G. W. Hammett, C. Kim, J. E. Kinsey, M. Kotschenreuther, A. H. Kritz, L. L. Lao, J. Mandrekas, W. M. Nevins, S. E. Parker, A. J. Redd, D. E. Shumaker, R. Sydora, and J. Weiland, *Physics of Plasmas* **7**, 969 (2000), <https://doi.org/10.1063/1.873896>.
- [61] M. Cao and P. H. Diamond, *Plasma Physics and Controlled Fusion* **64**, 035016 (2022).
- [62] Z. Williams, M. Pueschel, P. Terry, T. Nishizawa, D. Kriete, M. Nornberg, J. Sarff, G. McKee, D. Orlov, and S. Nogami, *Nuclear Fusion* **60**, 096004 (2020).
- [63] M. Hirsch, J. Baldzuhn, C. Beidler, R. Brakel, R. Burhenn, A. Dinklage, H. Ehmler, M. Endler, V. Erckmann, Y. Feng, J. Geiger, L. Giannone, G. Grieger, P. Grigull, H.-J. Hartfuß, D. Hartmann, R. Jaenicke, R. Kämpf, H. P. Laqua, H. Maaßberg, K. McCormick, F. Sardei, E. Speth, U. Stroth, F. Wagner, A. Weller, A. Werner, H. Wobig, and S. Z. and, *Plasma Physics and Controlled Fusion* **50**, 053001 (2008).
- [64] Y. Suzuki, *Plasma Physics and Controlled Fusion* **62**, 104001 (2020).
- [65] M. Bernert, T. Eich, A. Kallenbach, D. Carralero, A. Huber, P. T. Lang, S. Potzel, F. Reimold, J. Schweinzer, E. Viezzer, and H. Zohm, *Plasma Physics and Controlled Fusion* **57**, 014038 (2014).
- [66] A. Huber, M. Bernert, S. Brezinsek, A. Chankin, G. Sergienko, V. Huber, S. Wiesen, P. Abreu, M. Beurskens, A. Boboc, M. Brix, G. Calabro, D. Carralero, E. Delabie, T. Eich, H. Esser, M. Groth, C. Guillemaut, S. Jachmich, A. Järvinen, E. Joffrin, A. Kallenbach, U. Kruezi, P. Lang, C. Linsmeier, C. Lowry, C. Maggi, G. Matthews, A. Meigs, P. Mertens, F. Reimold, J. Schweinzer, G. Sips, M. Stamp, E. Viezzer, M. Wischmeier, and H. Zohm, *Nuclear Materials and Energy* **12**, 100 (2017), proceedings of the 22nd International Conference on Plasma Surface Interactions 2016, 22nd PSI.
- [67] A. V. Chankin and G. Saibene, *Plasma Physics and Controlled Fusion* **41**, 913 (1999).
- [68] R. Goldston, *Journal of Nuclear Materials* **463**, 397 (2015), pLASMA-SURFACE INTERACTIONS 21.

- [69] H. Sun, R. Goldston, A. Huber, X. Xu, J. Flanagan, D. McDonald, E. de la Luna, M. Maslov, J. Harrison, F. Militello, J. Fessey, and S. Cramp, *Nuclear Fusion* **61**, 066009 (2021).
- [70] D. Fernández-Ruiz, U. Losada, M. Ochando, B. Liu, C. Hidalgo, and the TJ-II Team, *Nuclear Fusion* **61**, 126038 (2021).
- [71] S. Sudo, Y. Takeiri, H. Zushi, F. Sano, K. Itoh, K. Kondo, and A. Iiyoshi, *Nuclear Fusion* **30**, 11 (1990).